FG03-85SF15798
DOE/SF/15798--T11

COMMUNITY GEOTHERMAL TECHNOLOGY PROGRAM

ELECTRODEPOSITION OF MINERALS IN GEOTHERMAL BRINE

Conducted by

Oceanit Laboratories, Inc.

1990

MASTER

DISTRIBUTION OF THIS DOCUMENT IS UNLIMITED

NOTICE

This report was prepared as an account of work sponsored by an agency of the United States Government. Neither the United States Government nor any agency thereof, nor any of their employees, makes any warranty, express or implied, or assumes any legal liability or responsibility for the accuracy, completeness, or usefulness of any information, apparatus, product, or process disclosed, or represents that its use would not infringe privately owned rights. Reference herein to any specific commercial product, process, or service by trade name, trademark, manufacturer, or otherwise, does not necessarily constitute or imply its endorsement, recommendation, or favoring by the United States Government or any agency thereof. The views and opinions of authors expressed herein do not necessarily state or reflect those of the United States Government or any agency thereof.

PREFACE

This is a report of work performed for the Community Geothermal Technology Program, a small grant program administered jointly by the Hawai'i Natural Energy Institute and the State of Hawai'i Department of Business, Economic Development and Tourism.

This project was one of five funded under the second phase of the program, which were awarded in 1988. Funds for this phase were provided by the U.S. Department of Energy, the County of Hawai'i, and donations from private business.

The opinions expressed in this reports are those of the author, and are not necessarily shared by the program administrators, funding agencies, or others involved in the program. Responsibility for the accuracy of the data provided in this report lies with the author.

The enthusiasm, talents, and efforts of the grantees are much appreciated, and I look forward to continuing to work with them and with future recipients of grants from the Community Geothermal Technology Program.

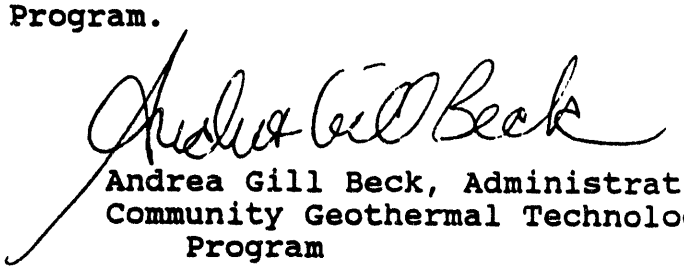

Andrea Gill Beck, Administrator
Community Geothermal Technology
Program

Hawai'i Energy Extension Service
Dept. of Business, Economic
Development and Tourism
99 Aupuni Street, #214
Hilo, HI 96720

TABLE OF CONTENTS

LIST OF TABLES

LIST OF FIGURES

I. INTRODUCTION

A. BACKGROUND

In early 1989 the Hawaii Energy Extension Service of the Department of Business, Economic Development and Tourism, Energy Division, together with the Hawaii Natural Energy Institute, sponsored Oceanit Laboratories, Inc. to perform experiments with geothermal brine from the HCP-A geothermal well at Puna, island of Hawaii (Figure 1). The grant totaled

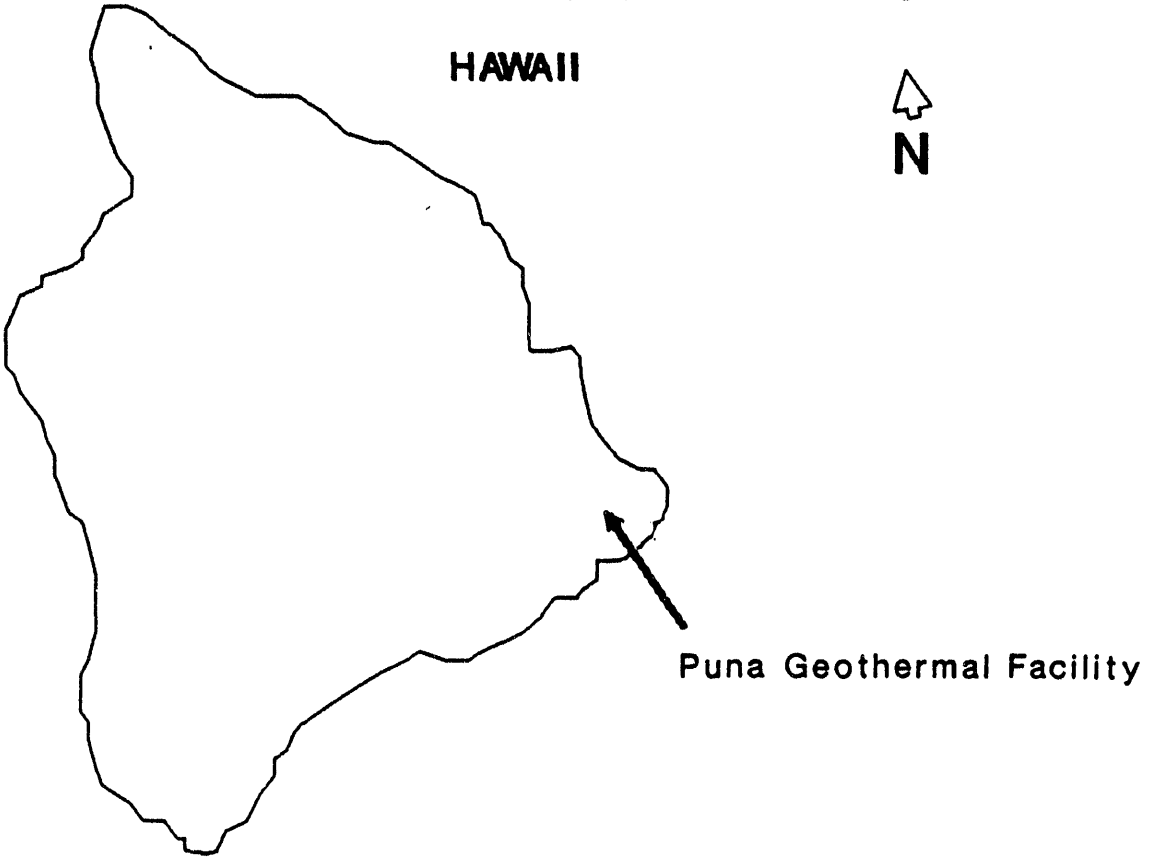

Figure 1. Location of experiment.

$8,421.90 and was part of the Community Geothermal Technology Program (CCGTP). Work was performed at the Noi'i O Puna geothermal laboratory operated by the Natural Energy Laboratory of Hawaii and located at its Puna Geothermal Facility.

The purpose of the CGTP is to identify alternative uses of geothermal brine that could provide an economic value. Geothermal brine contains dissolved minerals that can be electrolytically deposited onto an electrically charged substrate. Our interest in this project was to investigate opportunities to create small structures from electrolytically deposited material. This technology has been used to produce mineral layers over metal structures, thereby providing corrosion protection, as well as to create artificial reefs and other underwater structures.

Electrodeposition occurs when a potential is applied across a cathode and anode in an electrolyte, e.g., geothermal brine or seawater. The resulting potential difference induces a migration of ions through the electrolyte, enabling the depositing of certain ions at the cathode. Cations in the electrolyte, e.g., Ca^{2+} and other positive ions, reduce at the cathode, providing a protective coating. Previous investigations of electrodeposition in seawater found compressive strengths comparable to cement (Hilbertz 1979; Mitsui 1988). Figure 2 depicts the primary chemical processes expected to occur during electrodeposition in geothermal brine.

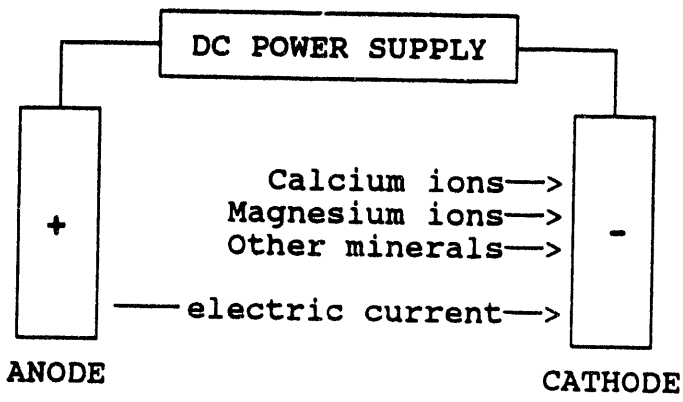

$2Cl^- \longrightarrow Cl_2(gas) + 2e^-$
$2H_2O \longrightarrow O_2(gas) + 4H^+ + 4e^-$

$H_2O + 2e^- \longrightarrow H_2(gas) + 2OH^-$
$O_2 + 2H_2O + 2e^- \longrightarrow 2OH^-$
$H_2CO_3 + H^+ + HCO_3^- \longrightarrow 2H^+ + CO_3^{2-}$
$Mg^{2+} + 2OH^- \longrightarrow Mg(OH)_2$ (brucite)
$Ca^{2+} + CO_3^{2-} \longrightarrow CaCO_3$ (aragonite)

Figure 2. Chemistry of electrodeposition.

Geothermal brine is similar to seawater except that it contains substantially more silica and substantially less magnesium and sulfates. However, concentrations of calcium are similar (for the HGP-A site). Table 1 provides a comparison of the minerals found in seawater and geothermal brine from the HGP-A well.

B. OBJECTIVE

The primary objective of this research was to determine the characteristics of materials produced via the electrodeposition of minerals in geothermal brine, with the expectation that aggregated materials could be employed as useful devices, e.g., park benches.

The research described herein investigates the characteristics of materials produced via electrodeposition of minerals in geothermal brine from the HGP-A well in Puna, Hawaii.

TABLE 1

Composition comparison of seawater and brine from HGP-A site.

CONSTITUENT	HGP-A BRINE	SEAWATER
Silica, SiO_2 (ppm)	860	4
Chlorine, Cl (ppm)	9,435	19,500
Sodium, Na (ppm)	5,245	9,600
Potassium, K (ppm)	645	398
Calcium, Ca (ppm)	450	450
Magnesium, Mg(ppm)	0.2	1,290
Sulfate, SO_4 (ppm)	25	2,200
pH	6.6	8.2
Salinity (ppt)	17	35

Note: Values taken from Community Geothermal Technology Program Proposal Solicitation.

II. METHODOLOGY

A. ELECTRODEPOSITION

The basic electrodeposition unit setup is diagrammed in Figure 3 and photographed in Figure 4.

The geothermal brine was obtained directly from the heat

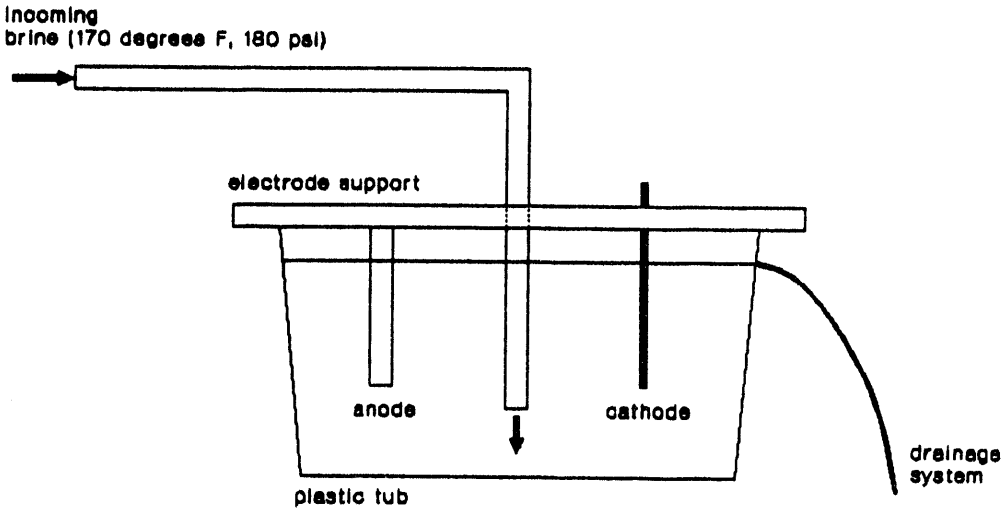

Figure 3. Diagram of electrodeposition unit.

exchanger in the geothermal laboratory, Noi'i O Puna, and was piped into three separate non-corrosive tubs at a temperature of approximately 170° F and a pressure of approximately 180 psi. Each plastic tub held approximately 170 liters (0.17 m^3) of brine and had a surface area of 1.49 m^2 in contact with the brine. The brine had a surface area of 0.37 m^2 in contact with the air. The flow rate of the brine into each tub was controlled by separate valves, which also allowed for further control over the equilibrium temperature of the brine. However, at higher flow rates the brine tended to become steam, and as a result, a flow rate of approximately 32 liters/hour was maintained. To accommodate the incoming brine, the tubs were drained as they overflowed through a 1/2" piece of Tygon tubing. Under these conditions, the temperature of the brine in the tubs was approximately 140° F.

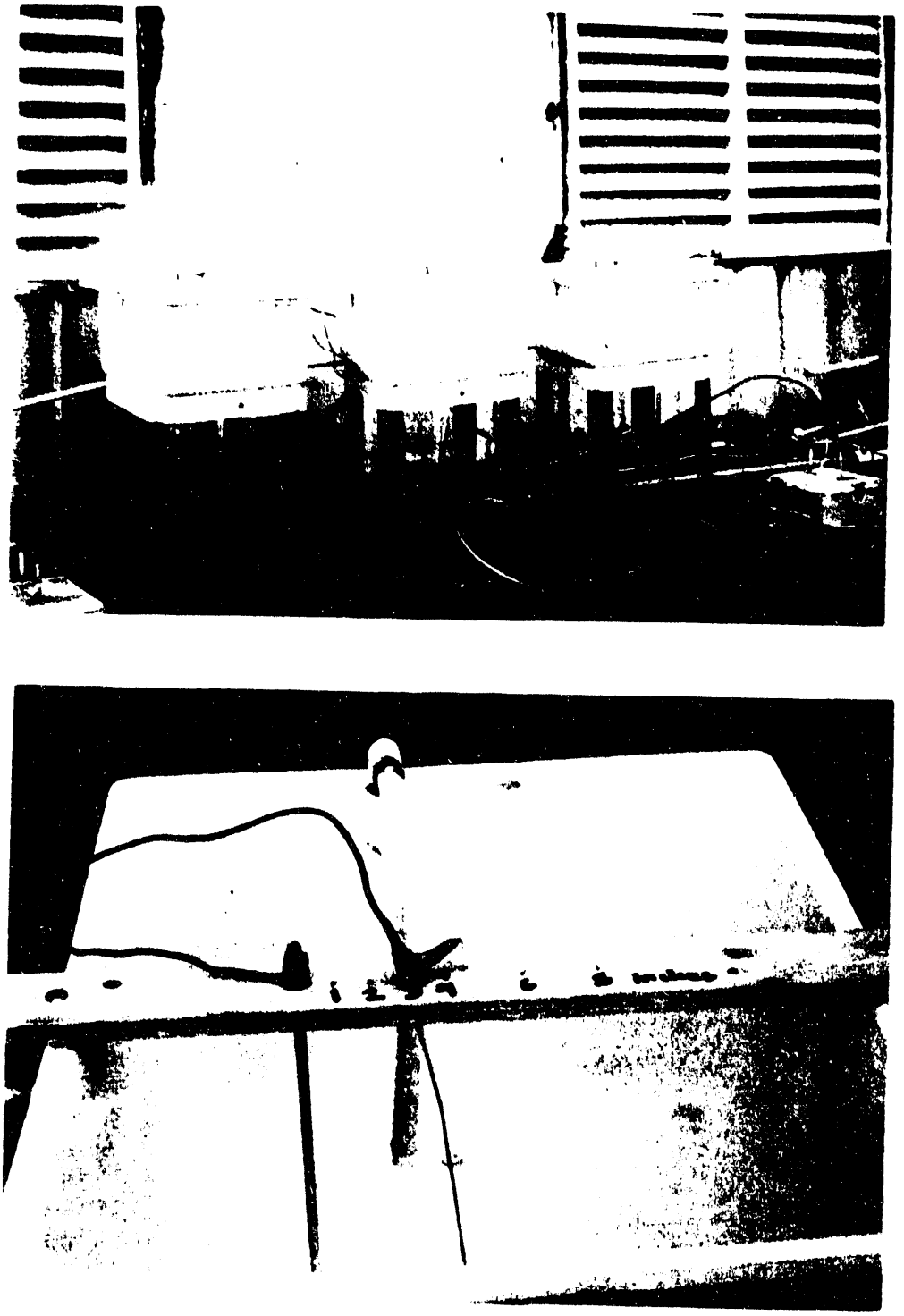

Figure 4. Photographs showing electrodeposition cell setup.

Initially a 30 cm by 2 mm stainless steel wire cathode and a 1.26 cm diameter threaded steel rod anode were suspended in the brine by wooden supports. Due to severe deterioration of the steel anodes, they were later replaced with carbon graphite anodes more resistant to corrosion. Several mounting sites on the supports allowed for a variety of electrode spacings. Identical electrodes were used in each of the three cells to minimize any effects of electrode size. A 20 VDC source supplied the voltage for the three parallel cells, with individual cell voltages further altered by load resistors. Table 2 lists the initial setup for each of the three cells. The cells were operated under these conditions for approximately thirty day intervals.

TABLE 2

Electrode spacing and current density for the three cells.

CELL	ELECTRODE SPACING (cm)	CURRENT DENSITY (A/cm^2)
1	7.5	0.7
2	7.5	7.4
3	7.5	14.3

Current density and cell resistance data were obtained using a Hewlett Packard 3421A Data Acquisition unit. An HP-71B mini-computer controlled the data acquisition process with results going to both a disk drive and printer. Figure 5 diagrams the general setup of the data acquisition system. Current and resistance data were taken every two hours during the experiment.

B. WEIGHT

Aggregates that formed at the cathodes were removed and sent to Oahu for analysis. Weights of the accumulated deposits were measured using a standard balance, Allied Fisher Scientific Scale Model 7224DA.

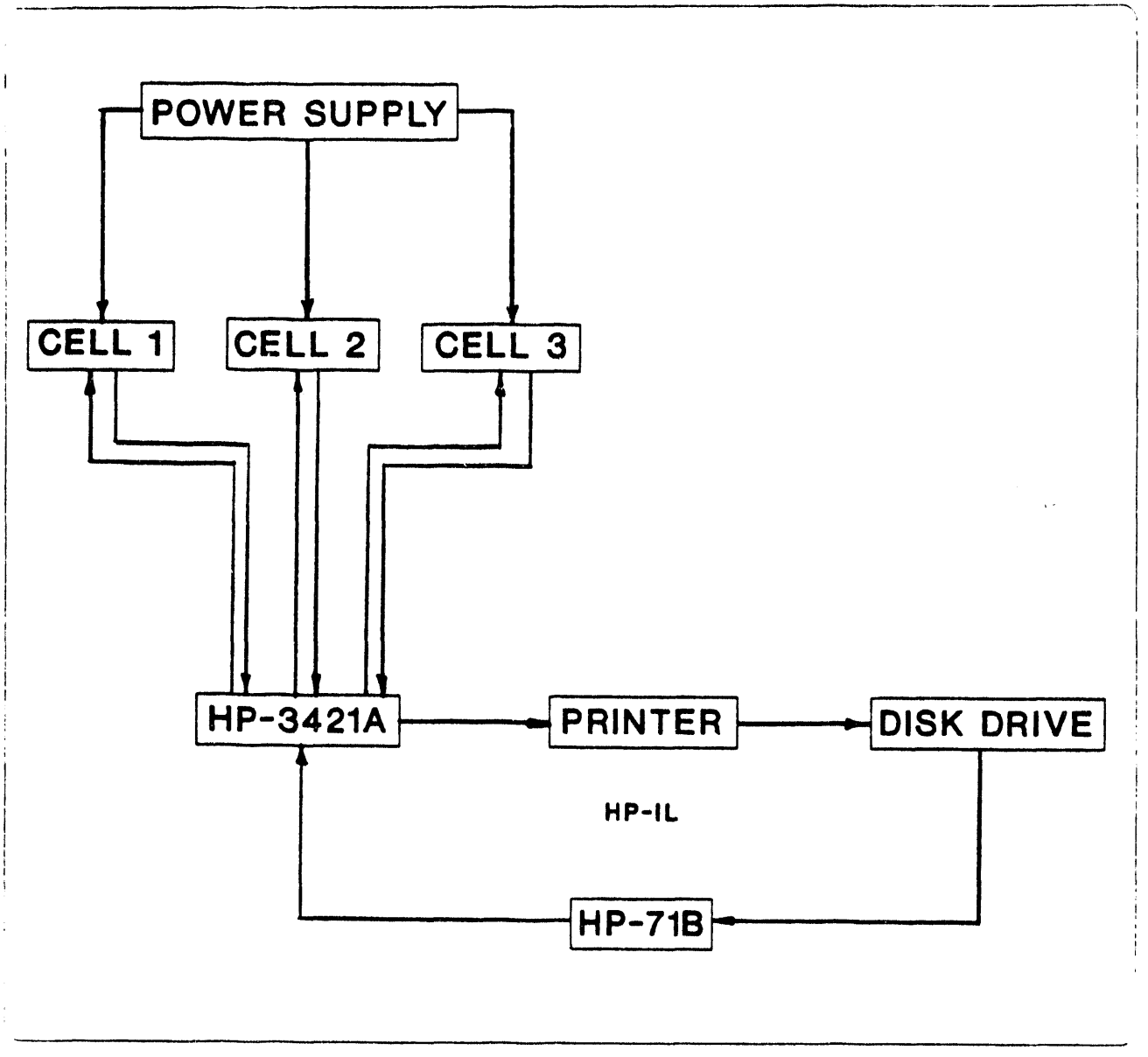

Figure 5. Schematic of data acquisition system.

C. CRYSTALLINE STRUCTURE

The crystalline structure of the deposits were determined using a Scintag PAD-V computer automated X-ray diffraction system (Cu K-alpha was used as the radiation source). The fundamentals of this technique involve recording the angle of diffraction from incident X-rays upon the sample. Using these angles, the atomic spacing and arrangement can be determined, thereby providing crystallographic information.

D. ELEMENTAL COMPOSITION

The elemental composition of the deposits were determined using a Princeton Gamma Tech System 4 plus SC System SS40 scanning electron microscope. Samples were attached to mounts with carbon paint; a 25 nm layer of carbon was sputtered on the aggregate surface. Scanning electron micrographs were taken at 500x and 1000x magnification. Elemental composition was determined using Energy Dispersive Spectroscopy (EDS) analysis.

III. RESULTS

Results are discussed principally for samples exposed during the last 30 days of our experiment. Results discussed also include an examination of precipitant from within the tub and from the region on the ground where the tubs drained. Samples from other than the last 30 days were not examined because they had been obtained using steel anodes, which experienced excessive deterioration.

A. ELECTRODEPOSITION

Visual examination of the electrodes indicate that higher current densities correspond to a greater accumulation of material upon the cathode. Traces from a photograph of the cathode showing the deposits are provided in Figure 6. The thickness of the accreted layer varied from 0.64 cm to 2.54 cm, with the greatest accumulation found on the cathode subjected to the highest current density. The deposited material was white and became powdery when dried. There were no visual differences among any of the three cathodes other than the thickness of deposited material. The sacrificial carbon graphite anodes experienced different degrees of deterioration: The anodes subjected to the medium and high current densities were flaky and had black strips breaking off, while the anode subjected to the low current density appeared relatively intact.

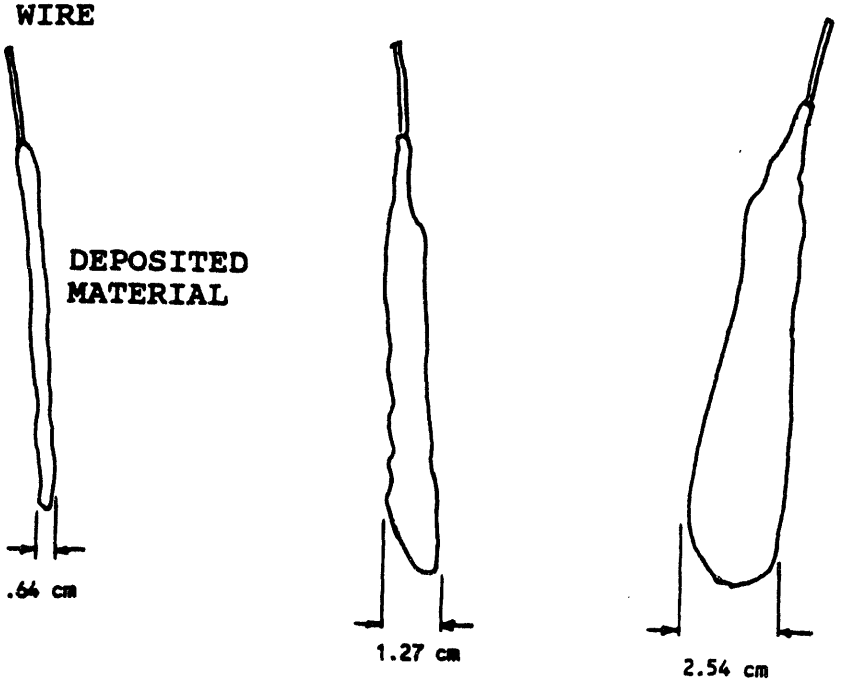

Figure 6. Sketch of accumulated deposit on each of the three electrodes (constructed from damaged photographs).

As mineral deposits accumulated on the cathodes, the cell currents and resistances remained relatively constant. The plot in Figure 7 shows the variation of current and resistance over time for the cell that experienced the greatest accumulation of deposited material. One would expect the resistance to increase as minerals deposited upon the cathode (increase in deposit thickness). Unfortunately, only seven days of data were available using graphite anodes because of power shortages (a temporary power shortage suspended data collection until the system could be reset). However, more extensive data from previous runs show the resistances increasing quickly after start up and eventually leveling off (Figure 8).

One problem encountered during the electrodeposition process was the precipitation of silica onto the sides of the tubs and electrodes as the temperature of the brine dropped below the saturation temperature. The white gel would accumulate several layers thick on the bottom and sides of the tubs, sometimes blocking the drainage of the brine through the Tygon tubing. This could perhaps be avoided by modifying the circulation system to drain the brine from the bottom of the tub, thereby flushing much of the precipitated silica out along with the draining fluid.

B. WEIGHT

The weights of deposits accumulated upon each cathode are shown in Figure 9. Cathodes subjected to higher current densities exhibited greater weight accumulation of the mineral deposits, consistent with visual observations.

C. CRYSTALLINE STRUCTURE

Table 3 lists the primary crystal structures found in each of the samples (Note: in addition to the crystalline structures indicated, each sample contained a certain amount of amorphous material believed to be silica). It is likely that

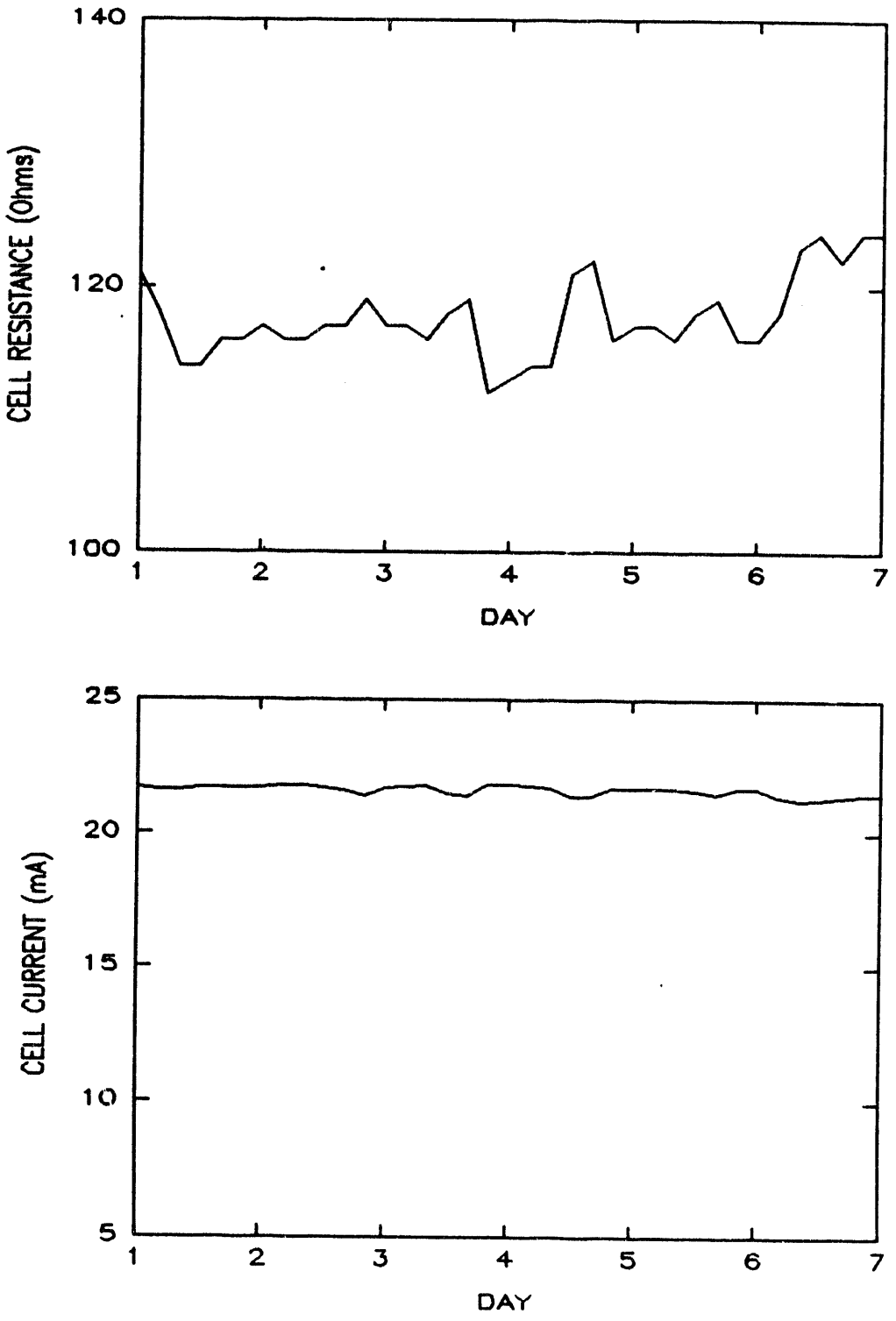

Figure 7. Change of resistance and current vs. time for cell subjected to high current density.

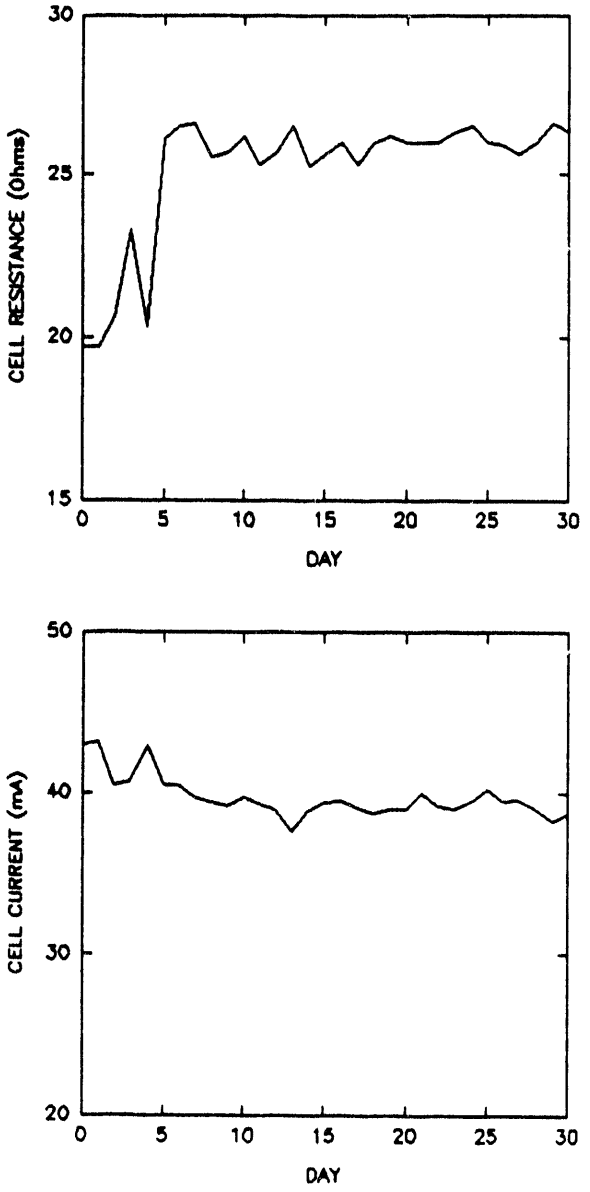

Figure 8. Change in resistance and current for a 30 day run of the cell using steel anodes.

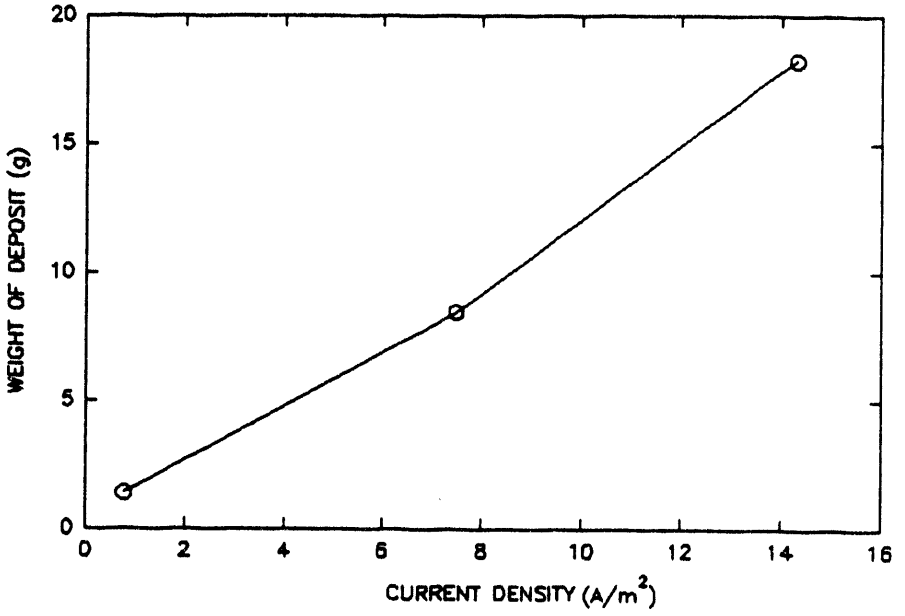

Figure 9. Weight vs. current density.

TABLE 3
Crystalline structure of samples.

COLLECTION SITE	GROUND	TUB	CATHODE #1 (low current)	CATHODE #2 (med. current)	CATHODE #3 (high current)
PRECIPITATE FOUND	halite am. silica	halite sylvite am. silica	halite vaterite calcite am. silica	halite vaterite calcite am. silica	halite vaterite calcite aragonite am. silica

the halite (HaCl) and sylvite (KCL) precipitated during evaporation of pore waters after samples were removed and allowed to dry. It is interesting to note the sequence of carbonate minerals precipitated under increasing current

density; it appears that vaterite forms first, followed by calcite and perhaps aragonite. Vaterite, calcite, and aragonite are all polymorphs of $CaCO_3$, with calcite being the most stable form. Vaterite and aragonite are both metastable with respect to calcite and will revert to that form under the proper conditions (Carlson). The variation of crystal structure with respect to current density suggests that the particular crystalline forms could be selectively deposited through regulation of the current density. Research performed in seawater found that aragonite was the most desirable polymorph of calcium because it offered the greatest compressive strength (Mitsui). Figure 10 shows an individual plot of the x-ray diffraction results, including the relative amounts of crystalline material (more extensive results are in Appendix B).

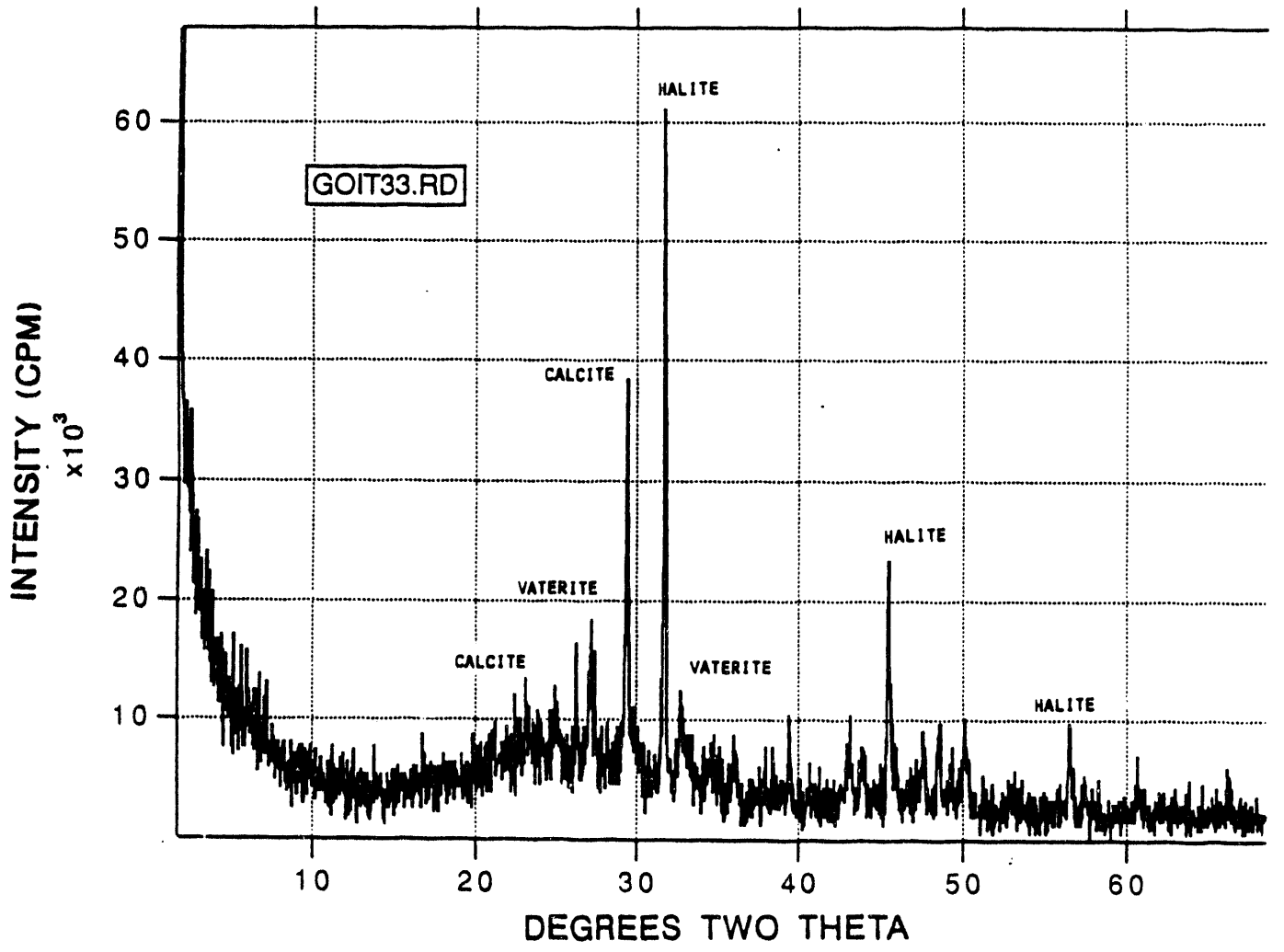

Figure 10. X-ray diffraction results for material deposited on high current density cathode (no.3). Results show relative amounts of crystalline material.

D. ELEMENTAL COMPOSITION

Results from Scanning Electron Microscopy (SEM) analysis of the samples indicate a relationship between magnitude of current density and minerals deposited. Samples collected from the ground consisted primarily of silica, with only trace amounts of calcium, potassium, and chlorine. Samples collected from the bottom of the tubs were also largely silica, but also contained significant amounts of chlorine. In several cases the amounts of chlorine in these samples exceeded the amount of silica.

Analysis from samples of material deposited on the cathodes indicated that as the current density increased, the relative amount of metallic cations, such as calcium, sodium, and potassium, also increased. It appears as if the moderate current density was most selective toward calcium while the higher current density tended to incorporate significant amounts of chlorine as well. This is likely to be the result of a process separate from that of electrodeposition, as chlorine is a negative ion and would be expected to accumulate on the anode and not on the cathode. Figures 11 and 12 are the results of the SEM and EDS analysis for the sample obtained from the high current density cathode (more extensive results are in Appendix A).

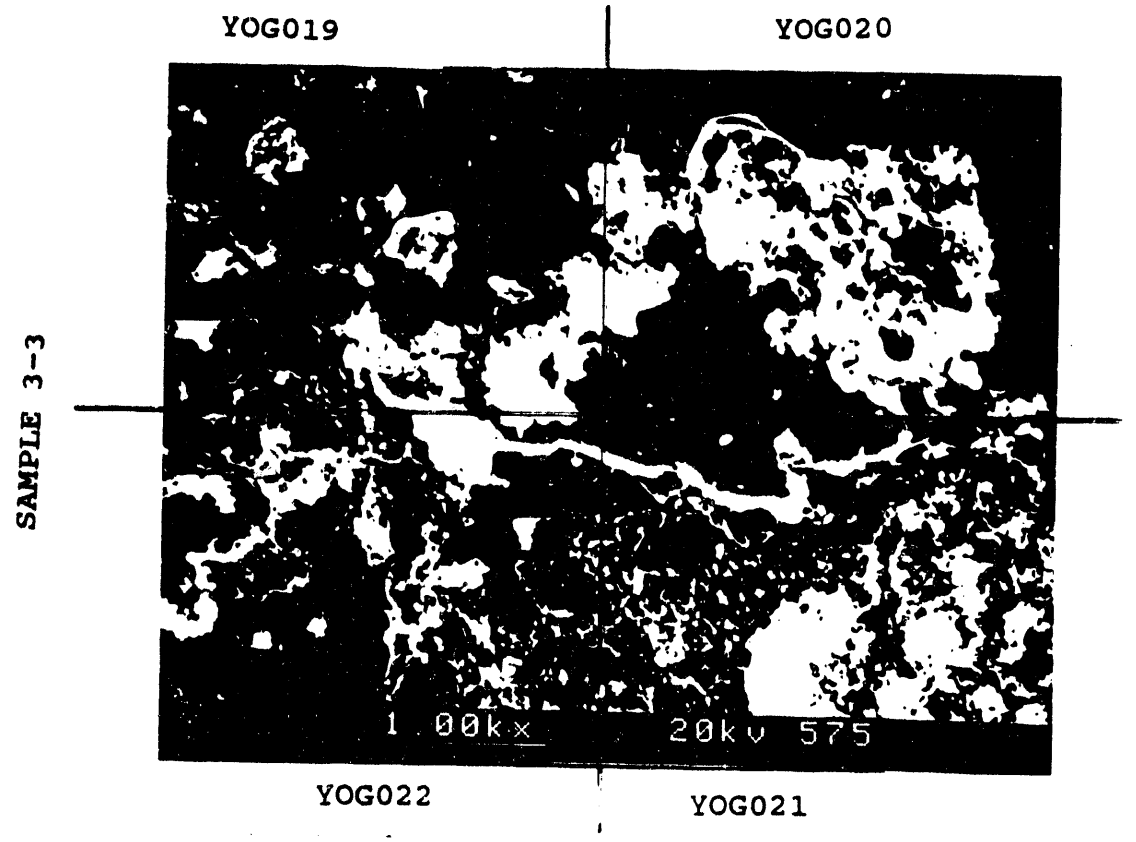

Figure 11. Scanning Electron Micrograph (SEM) results for high current density cathode. Energy Dispersive Spectroscopy (EDS) results for each SEM quadrant are provided in Appendix A. SEM enable us to obtain a detailed qualitative view of the sample under investigation. Comparisons between major physical features, together with elemental composition information, provide a more complete interpretation of results.

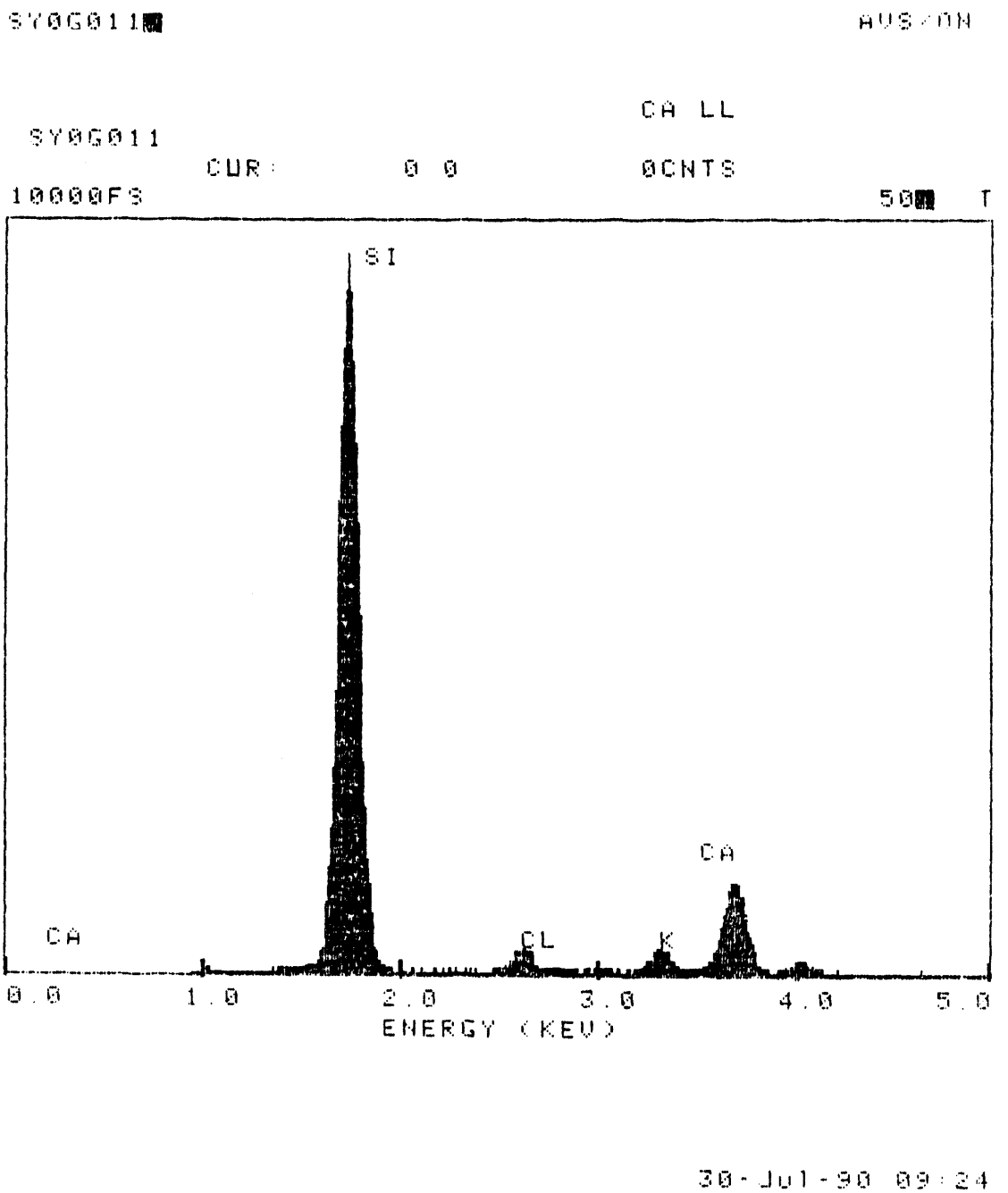

Figure 12. Results from Energy Dispersive Spectroscopy analysis (EDS). Peaks mark concentrations of certain elements, e.g., SI=Silicon, CA=Calcium, etc. Further results are in Appendix A.

IV. DISCUSSION

Due to limited time and resources we were only able to obtain one "good" set of electrolytically deposited material. Periodic interruptions of power also introduced additional variables into our experiment. However, much was learned from the experience of constructing and operating the experiment in the geothermal environment. This will prove valuable during future experiments.

Crystallographic analysis indicates that vaterite forms first, followed by calcite, and then perhaps aragonite as current density is increased. It would be desirable to perform further experiments in this area to determine potentials that selectively deposit the most desirable crystallographic forms.

Comparable results from electrodeposition experiments in seawater are available. In this case research occurred over several years concerning artificial reef structures and protective pile jackets created by electrolytically depositing minerals from seawater. Our results were similar to those found for seawater, e.g., deposit weights increased with current density, and composition changed with current density. Our experiment used current densities of approximately 0.76 to 1.4 mA/cm^2. Seawater researchers reported current densities varying from 0.11 mA/cm^2 to 700 mA/cm^2.

The correlation between rate of deposition and current density is in Figure 13. Assuming electricity costs $0.12 per kilowatt-hour, we can estimate an average cost per unit weight of 0.02 cents per gram. Creating a 2.5 kg block that could possibly be used for construction would therefore cost approximately 50 cents.

Interestingly, the accreted mass to expended power ratio for the geothermal brine was almost 150 times a typical value for seawater electrodeposition (Hilbertz encountered 1.9 kg of accreted mass per expended kW, while in this case the value exceeded 300 kg of accreted mass per kg)(Hilbertz 1979). A likely cause for the difference is the significant amount of silica found in samples deposited from the brine. In many cases silica was the major contributor to the mass of the sample; therefore, it is hard to make comparisons between the two results.

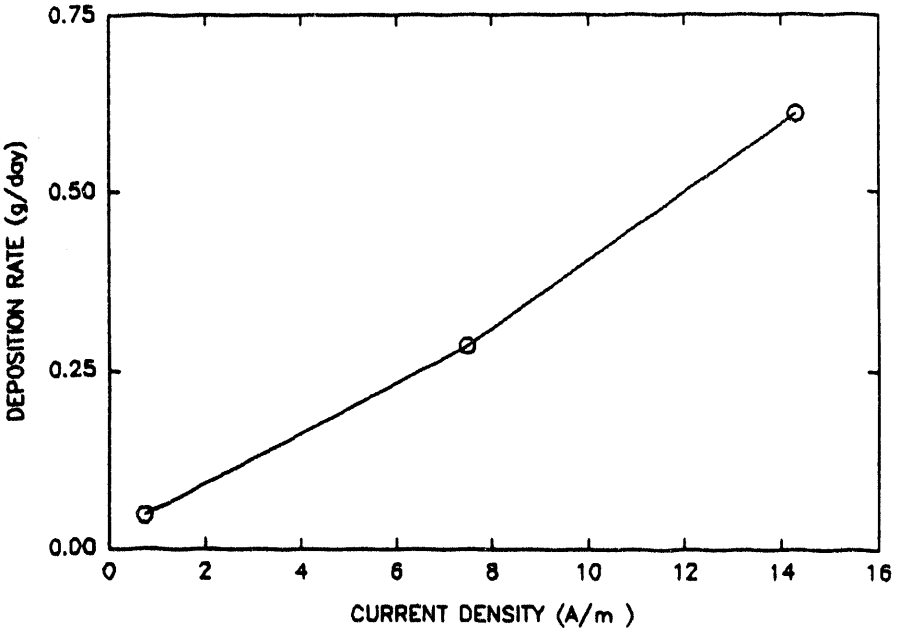

FIGURE 13. Rate of deposit vs. current density shows deposit rate increasing with current density.

While the cost-to-weight ratio appears reasonable, the slow rate of deposition in this experiment must be taken into consideration. At even the highest rates of deposition in this experiment, the time it would take to accumulate 2.5 kg exceeds 10 years. Assuming an increase in current density produces a proportional increase in rate of deposition (Mitsui found this to be the case in seawater)(Mitsui 1988), the current density would have to be increased by a factor of 4000 to accumulate 2.5 kg in a single day. A more practical solution would be to increase both the total cathodic surface area and the current significantly. This would give the ions more sites on which to deposit, thereby increasing the rate of deposition.

Another problem that must be considered is the precipitation of silica within the tubs. All of the electrolytically deposited samples contained significant amounts of silica in addition to the desired minerals, which most likely would effect the overall strength of the deposit. One possible solution is to maintain the temperature of the

brine above the saturation temperature of silica at all times. This, however, might require additional equipment or handling that could increase the cost of the electrodeposition process. Another possible solution would be to precipitate the silica before using the brine in the electrodeposition process. To do so, however, would essentially reduce the brine to a solution with even fewer minerals than seawater (Table 1), which is already a much more extensive and widely available resource.

Even though we installed a relatively sophisticated data acquisition system, we do not have a complete set of current and voltage measurements that correspond to weight accumulation. Preparations will have to be made in the future to accommodate for the possibilities of power shortages and other unforseen events.

We originally planned to investigate compressive strength characteristics of deposited materials with respect to crystalline structure and composition. However, samples taken became brittle and crumbly after they dried. Additionally, due to technical and logistical problems, we only aggregated one set (3 electrodes) of "good" samples.

Results from similar experiments performed in seawater found compressive strengths up to 4300 psi (Hilbertz 1979). Compressive strength of deposited materials formed in geothermal brine should be considered in future investigations, i.e., further investigations may yield techniques to reduce brittleness.

V. CONCLUSION

Electrodeposition in geothermal brine provides an interesting opportunity for the selective removal of minerals from the brine. However, more research is needed, including composition and weight with respect to current density, electrode configurations and spacings, and temperature effects on the electrodeposition process as well as artifacts produced from the presence of silica.

Practical uses of electrodeposited materials, e.g., building blocks, tables, benches, etc., could develop as technical questions regarding strength characteristics and deposition phenomenon become better understood.

VIII. SCHEDULE

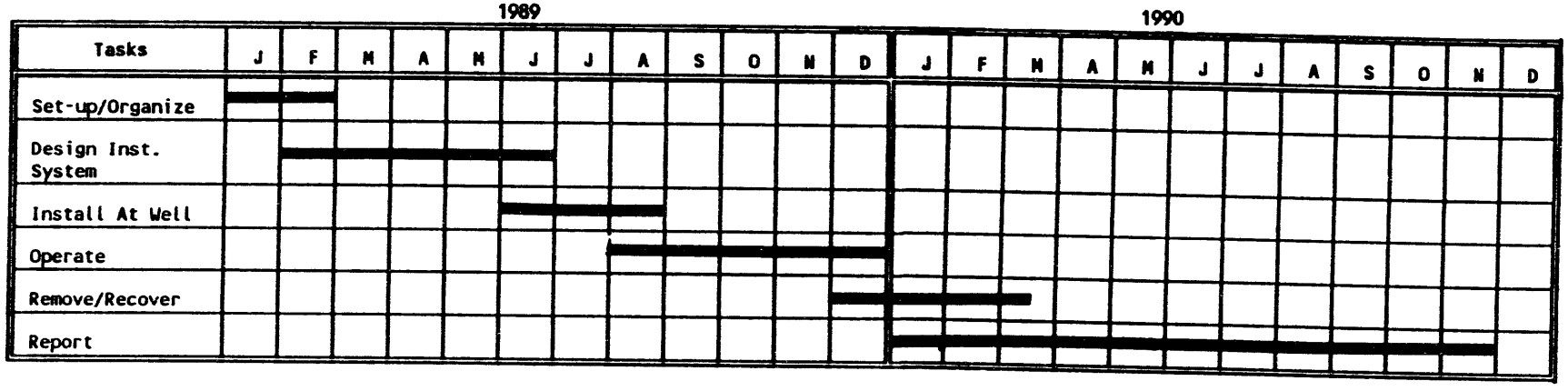

BIBLIOGRAPHY

Carlson, W.D. 1983, (11): 191-225. "The Polymorphs of $CaCO_3$ and the Aragonite-Calcite Transformation" Reviews in Mineralogy.

Gravens, Mark B. 1988, 14 (4): 519-530. "Electrodeposited Minerals in Marine Structures", Journal of Waterway, Port, Coastal, and Ocean Engineering, July.

Hilbertz, Wolf H. 1979, OE-4 (3): 94-112. "Electrodeposition of Minerals in Sea Water: Experiments and Applications," IEEE Journal on Oceanic Engineering, July.

Korlipara, Ravi. 1983, 17 (4): 19-28. "The Properties of Electrodeposited Minerals in Seawater," MTS Journal.

Mitsui Shipbuilding 1988. Internal Document.

Morse, John W. 1983, (11): 227-64. "The Kinetics of Calcium Carbonate Dissolution and Precipitation," Reviews in Mineralogy.

Wolfson, S.L. 1981, 32 (2): 70-76. "An Initial Investigation of Calcareous Deposits Upon Cathodic Steel Surfaces in Sea Water," Corrosion.

APPENDIX A

Energy Dispersive Spectroscopy (EDS) Results/Scanning Electron Microscopy (SEM)

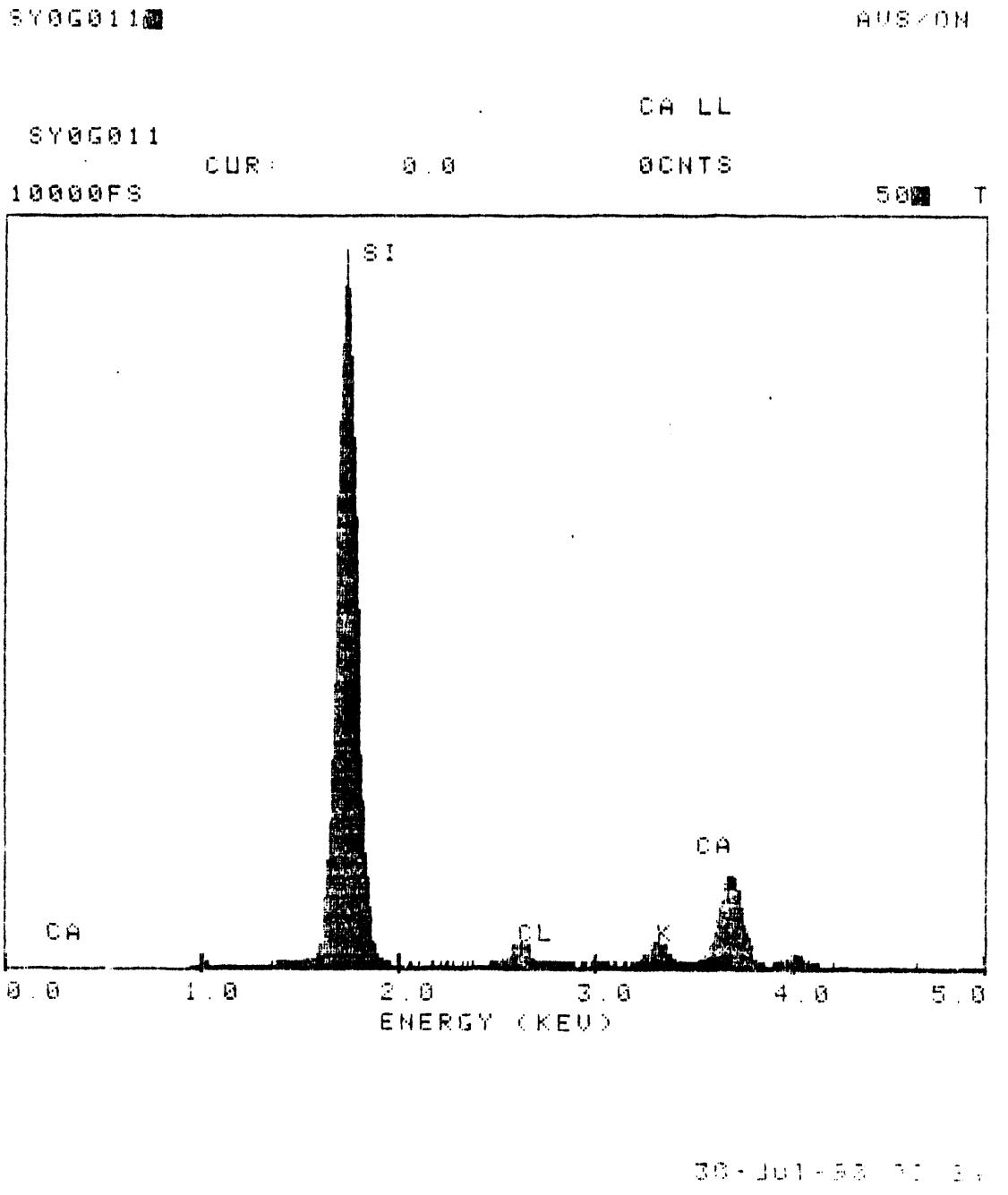

Figure A-1. Results from Energy Dispersive Spectroscopy (ED analysis for low current density cathode, SEM given in Figure 3-

Sample 3-1

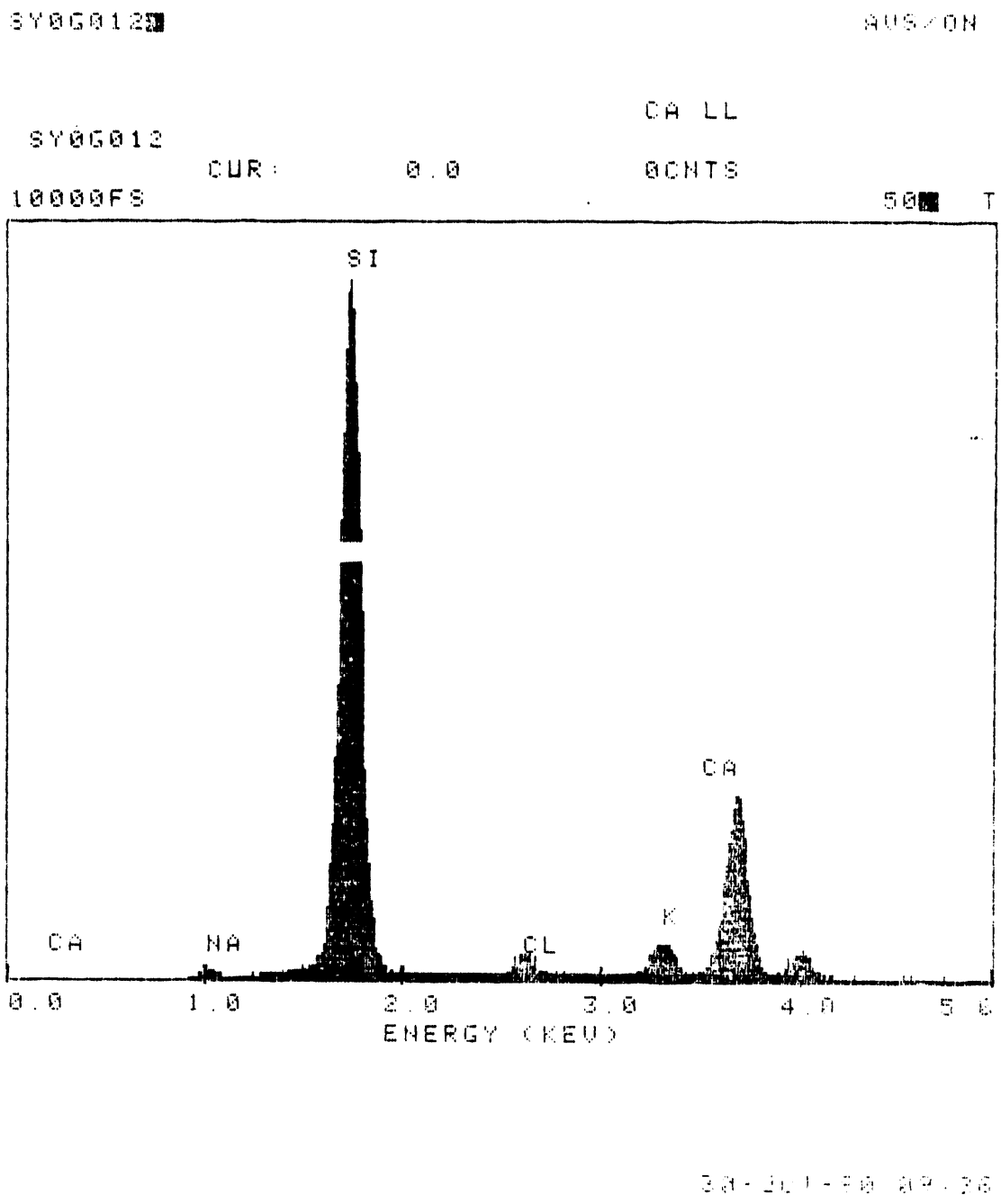

Figure A-2. Results from EDS analysis for low current densit cathode, SEM given in Figure 3-1.

Sample 3-1

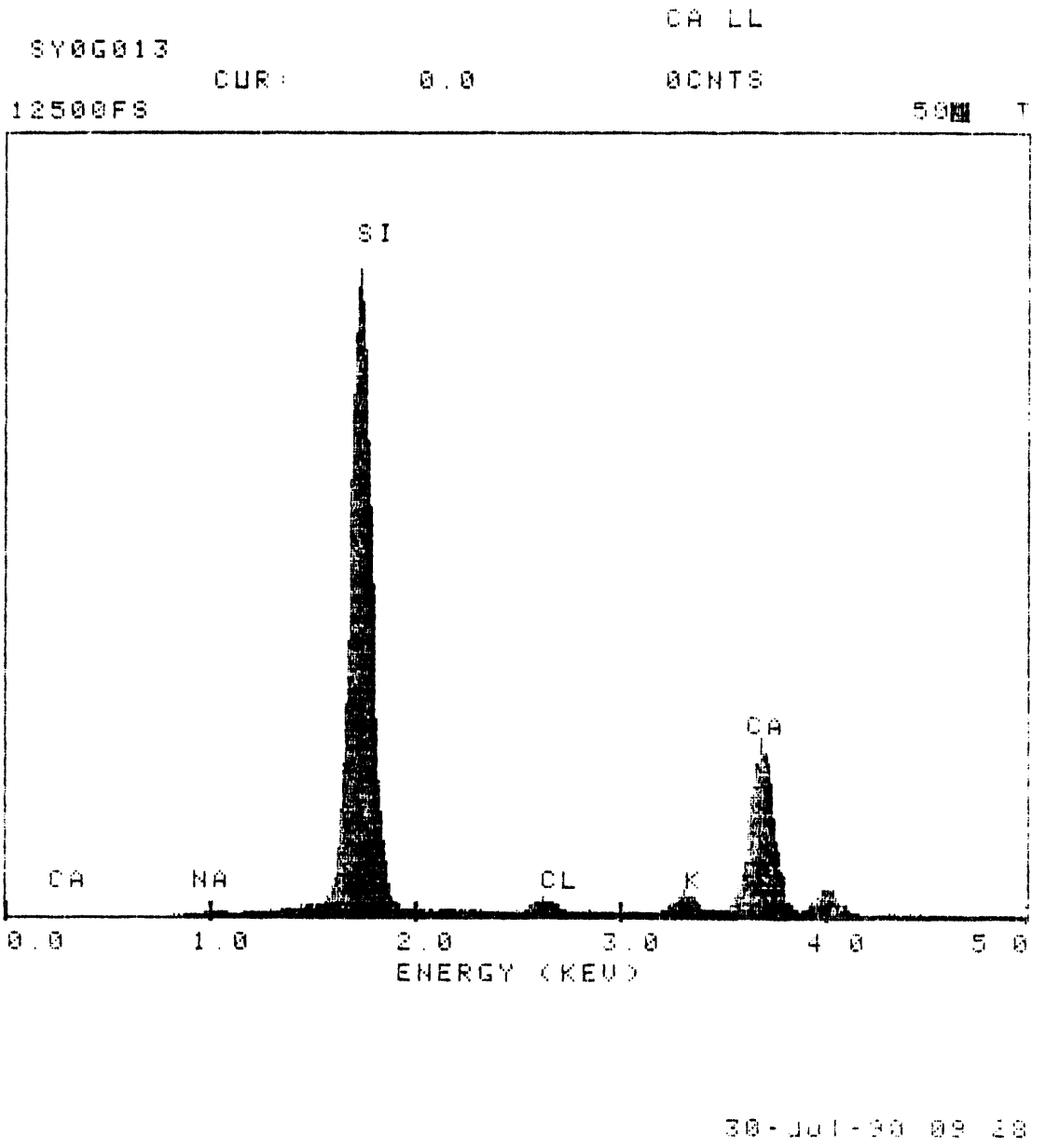

Figure A-3. Results from EDS analysis for low current density cathode, SEM given in Figure 3-1.

Sample 3-1

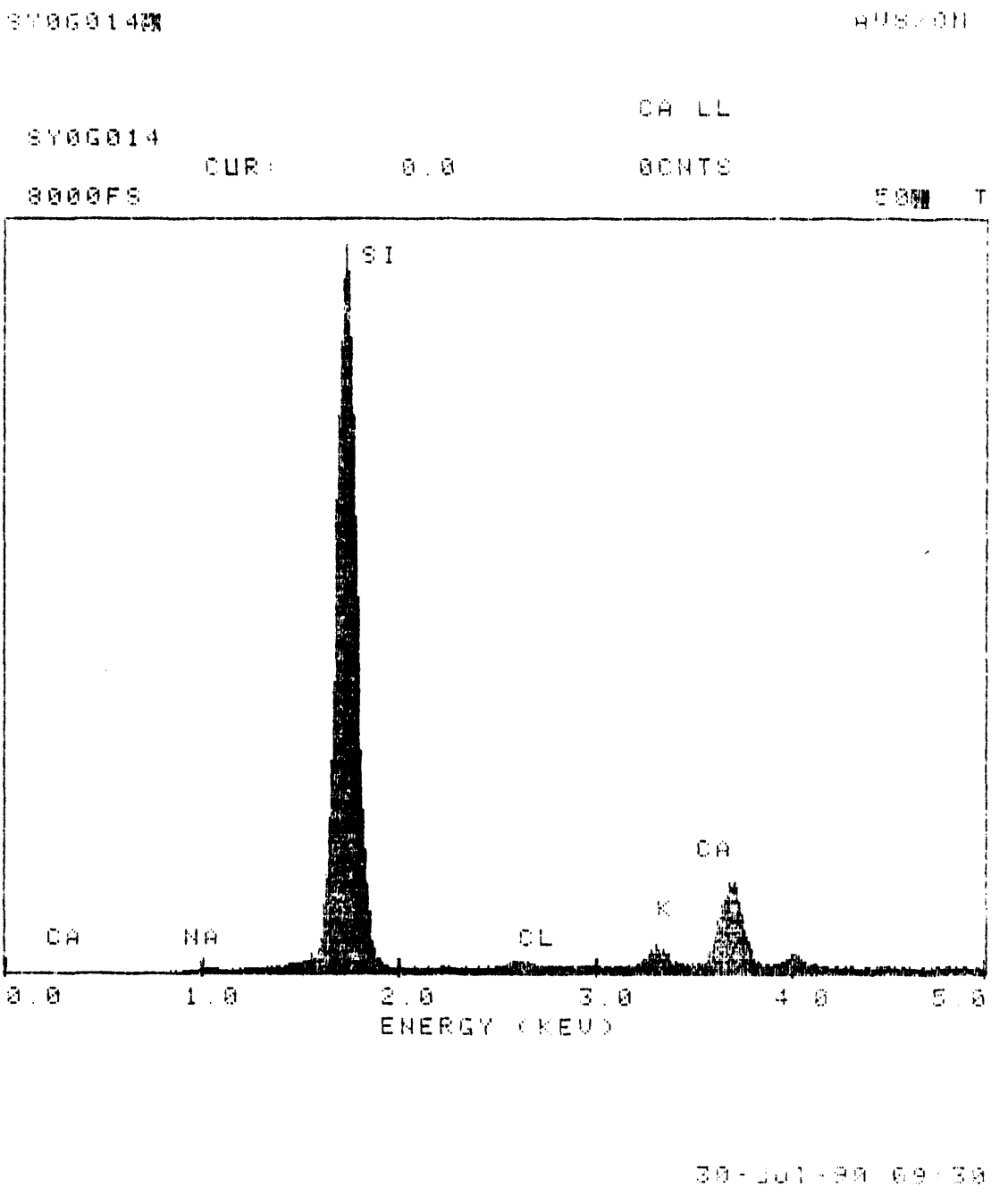

Figure A-4. Results from EDS analysis for low current density cathode, SEM given in Figure 3-1.

Sample 3-1

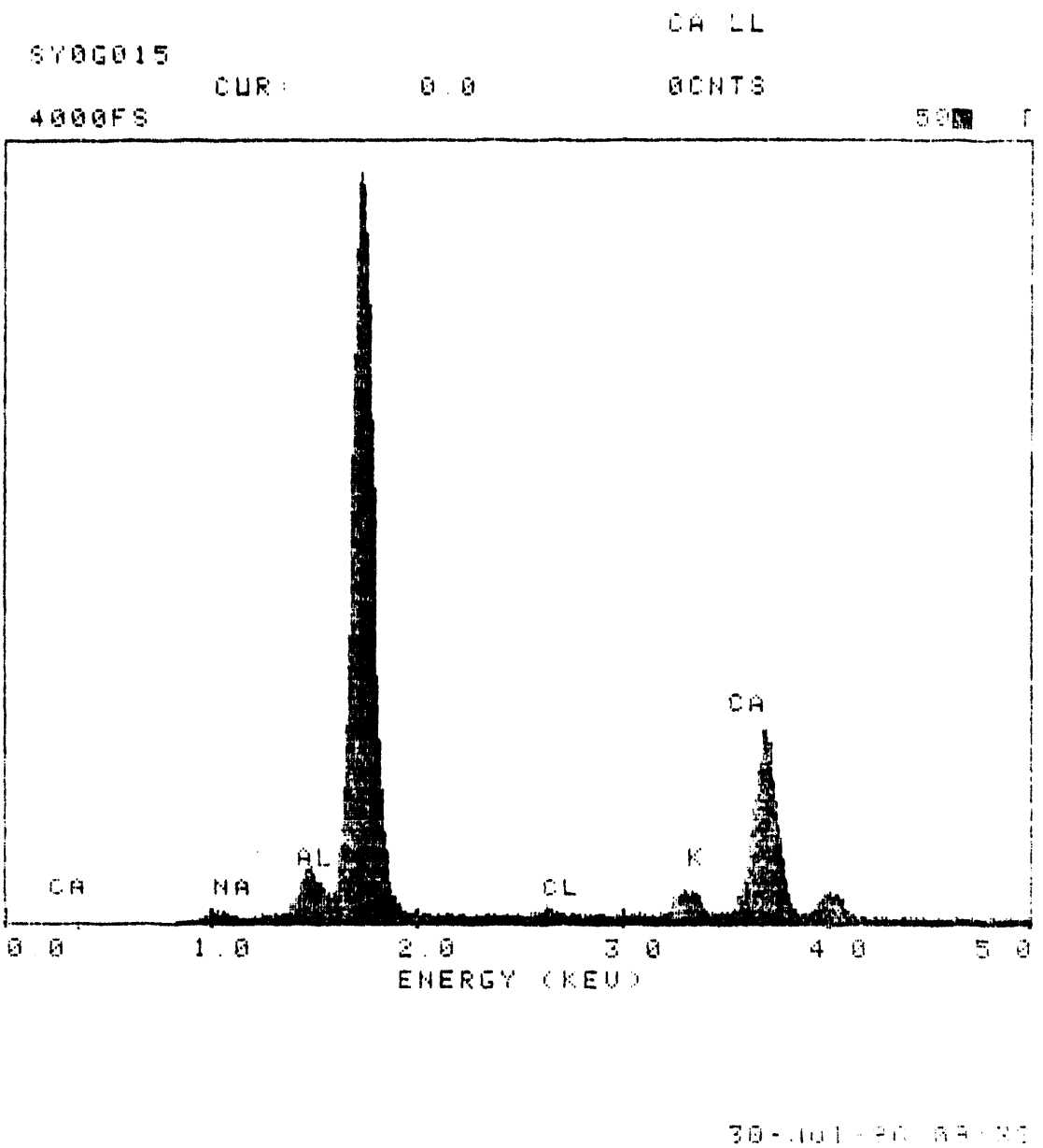

Figure A-5. Results from EDS analysis for medium current density cathode, SEM given in Figure 3-2.

Sample 3-2

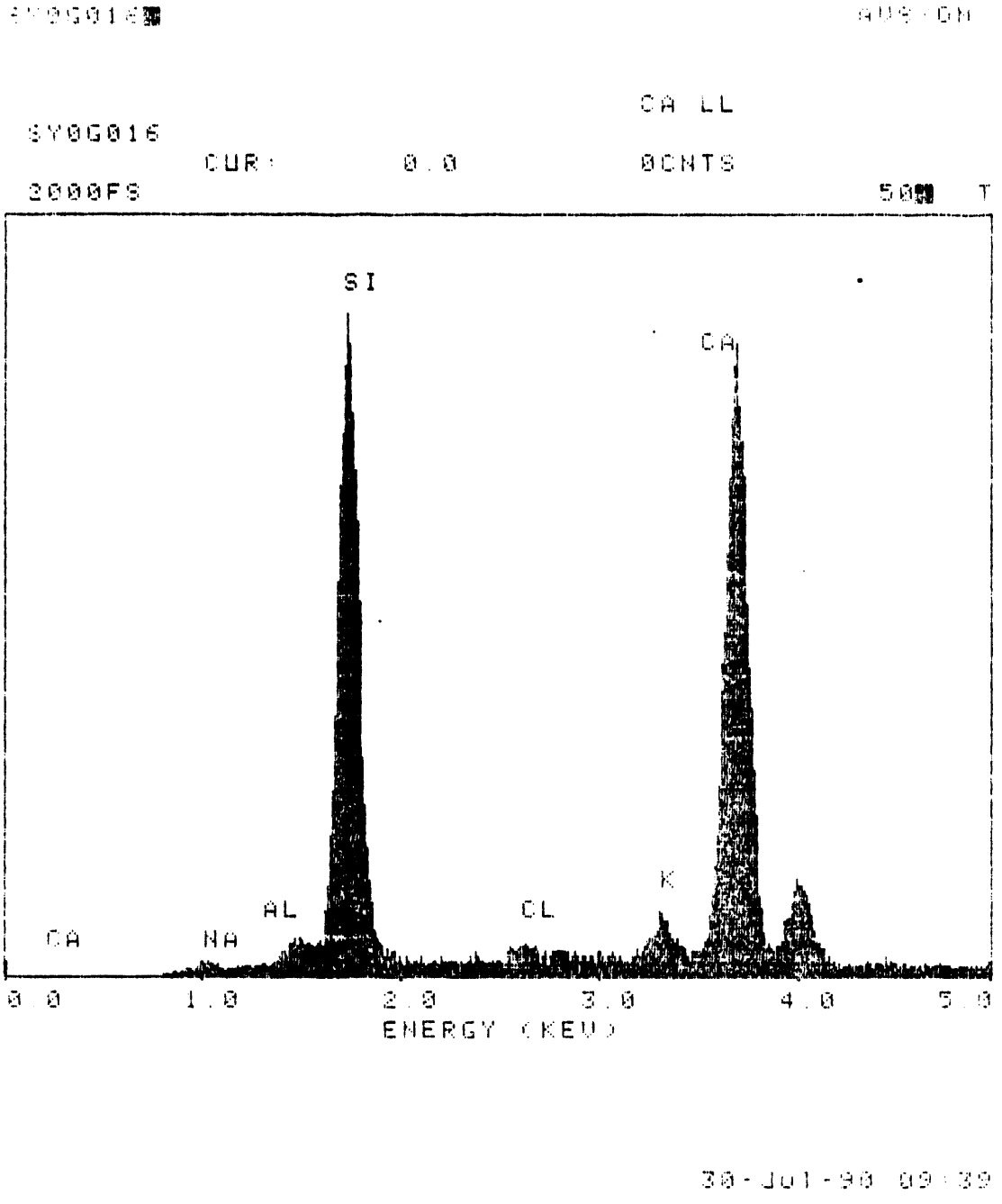

Figure A-6. Results from EDS analysis for medium current density cathode, SEM given in Figure 3-2.

Sample 3-2

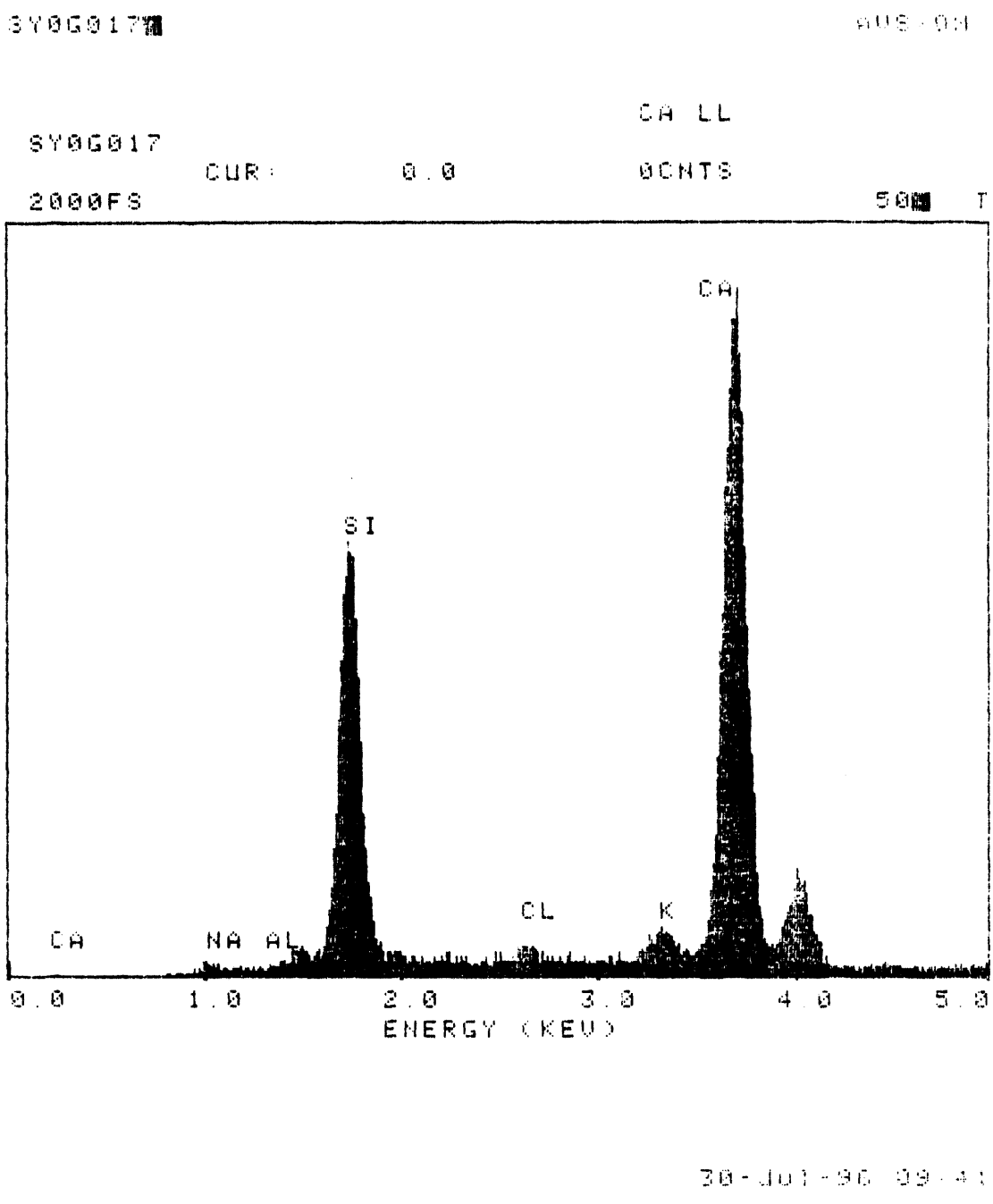

Figure A-7. Results from EDS analysis for medium current density cathode, SEM given in Figure 3-2.

Sample 3-2

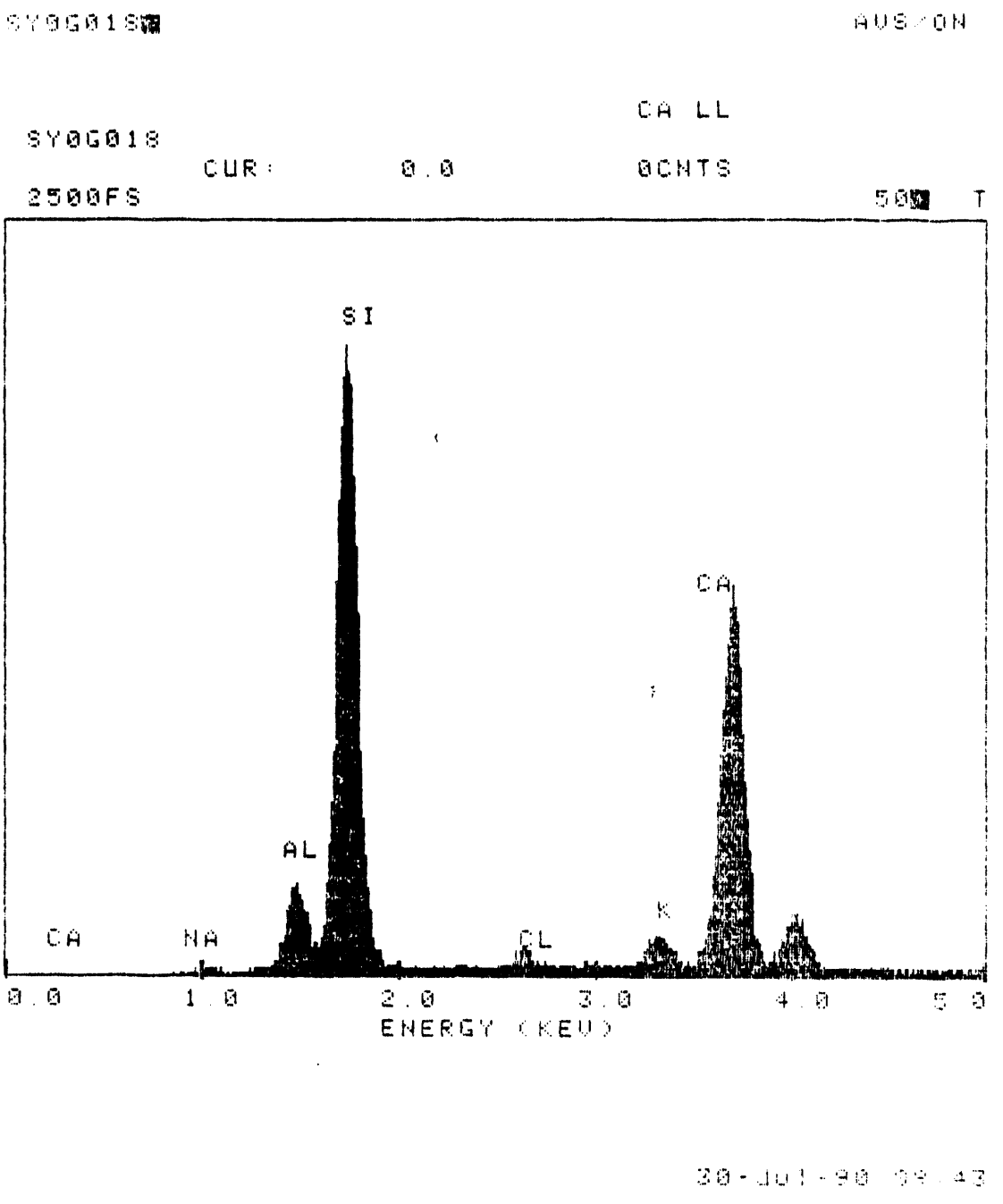

Figure A-8. Results from EDS analysis for medium current density cathode, SEM given in Figure 3-2.

Sample 3-2

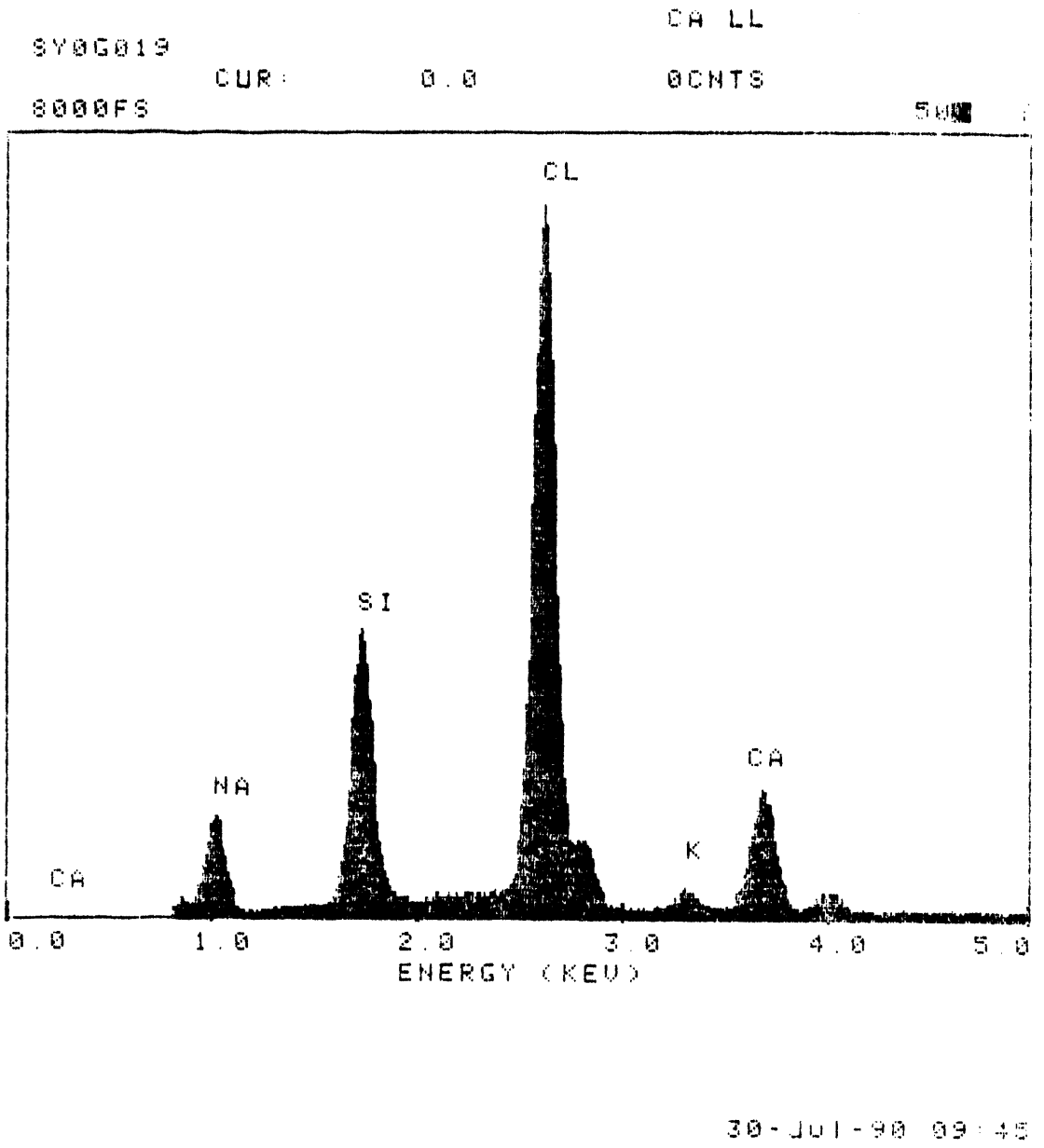

Figure A-9. Results from EDS analysis for high current density cathode, SEM given in Figure 3-3.

Sample 3-3

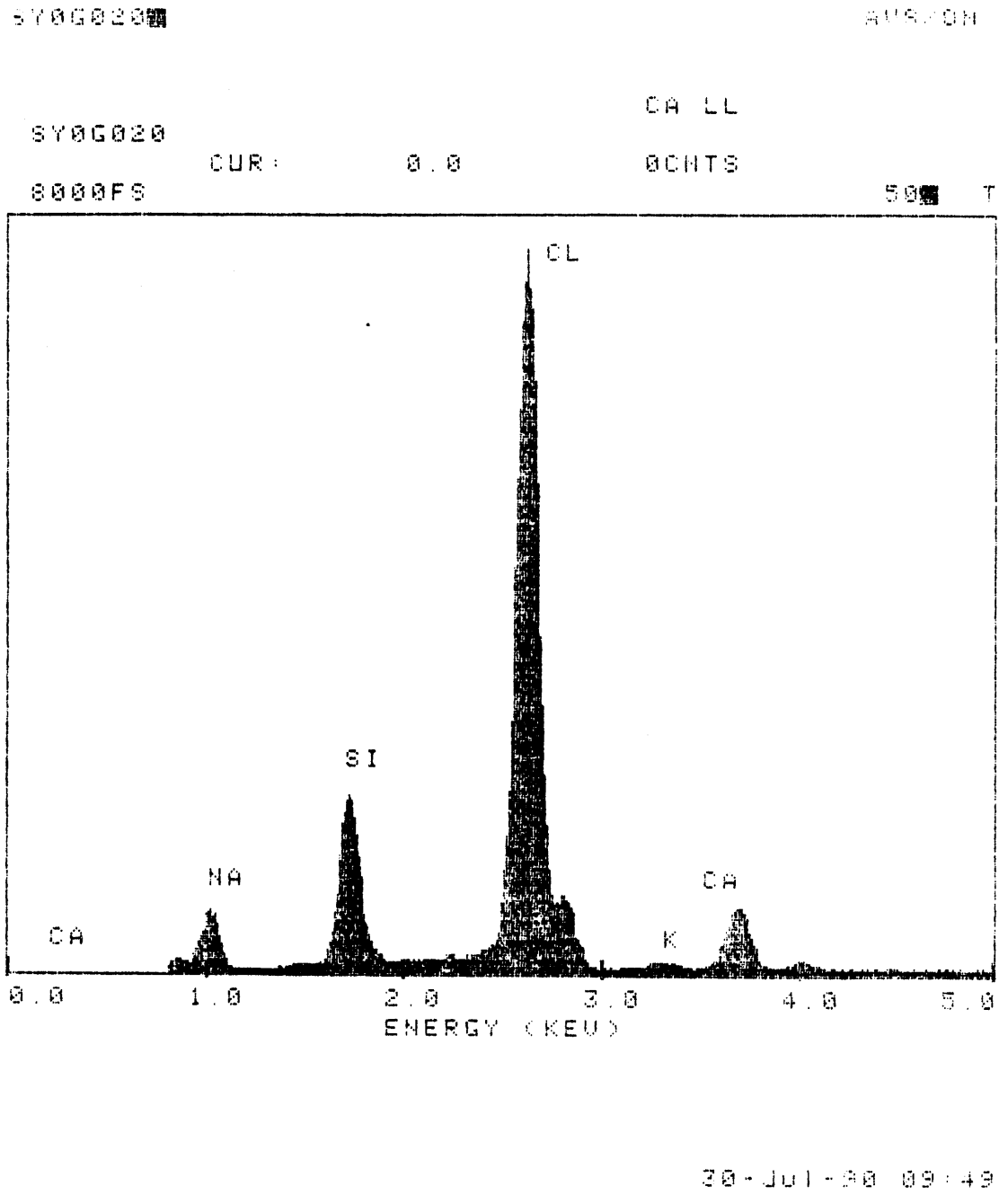

Figure A-10. Results from EDS analysis for high current density cathode, SEM given in Figure 3-3.

Sample 3-3

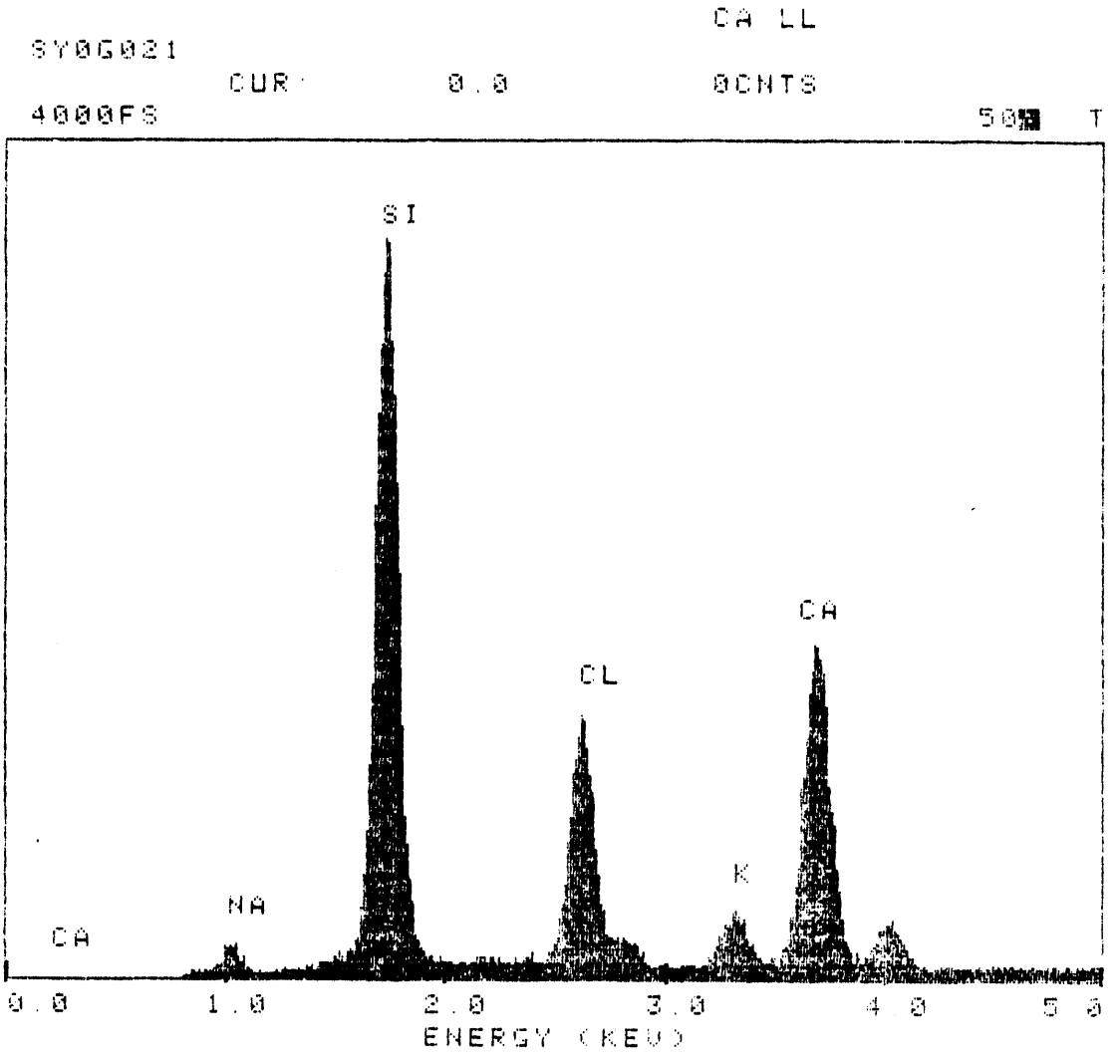

Figure A-11. Results from EDS analysis for high current density cathode, SEM given in Figure 3-3.

Sample 3-3

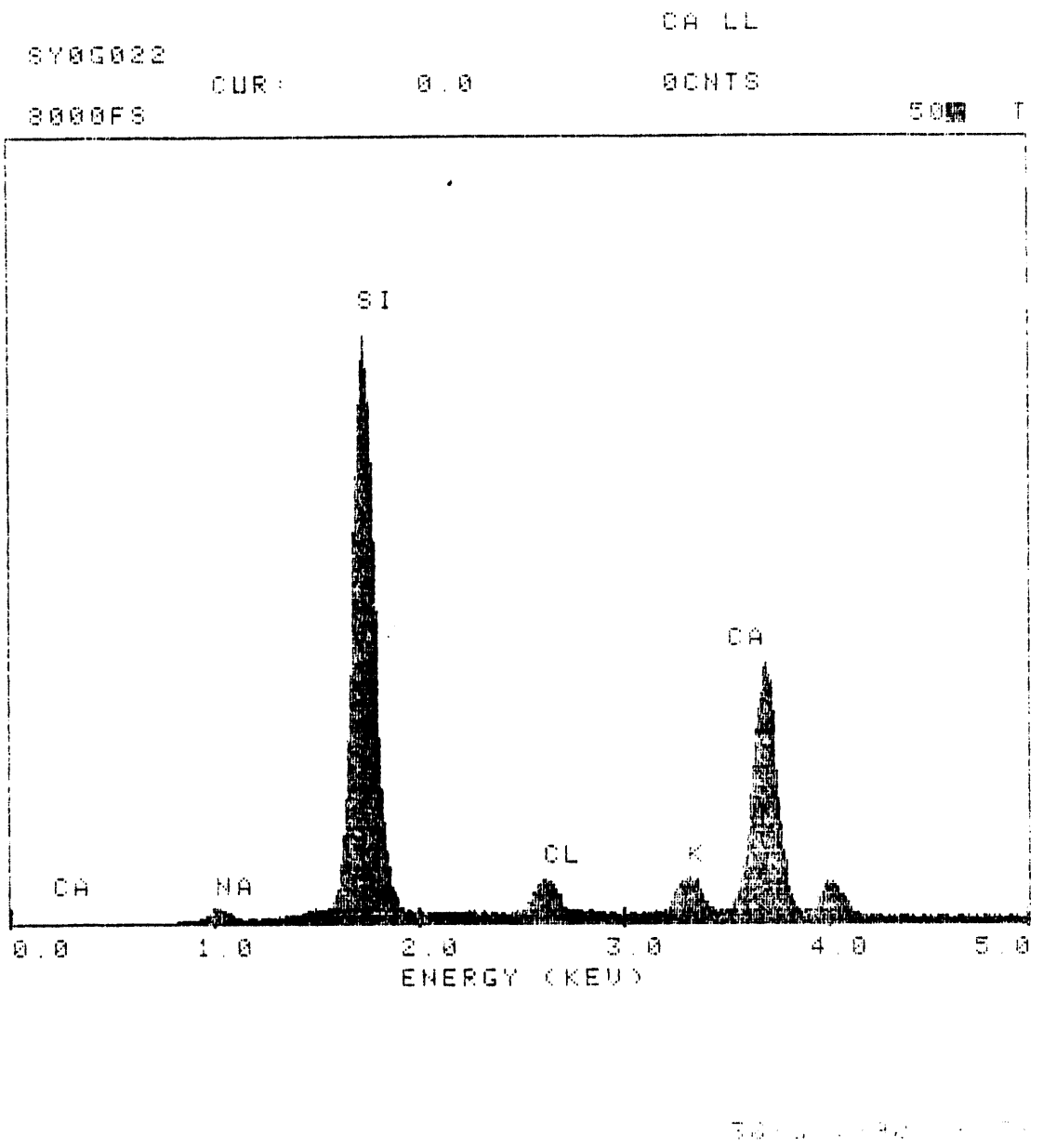

Figure A-12. Results from EDS analysis for high current density cathode, SEM given in Figure 3-3.

Sample 3-3

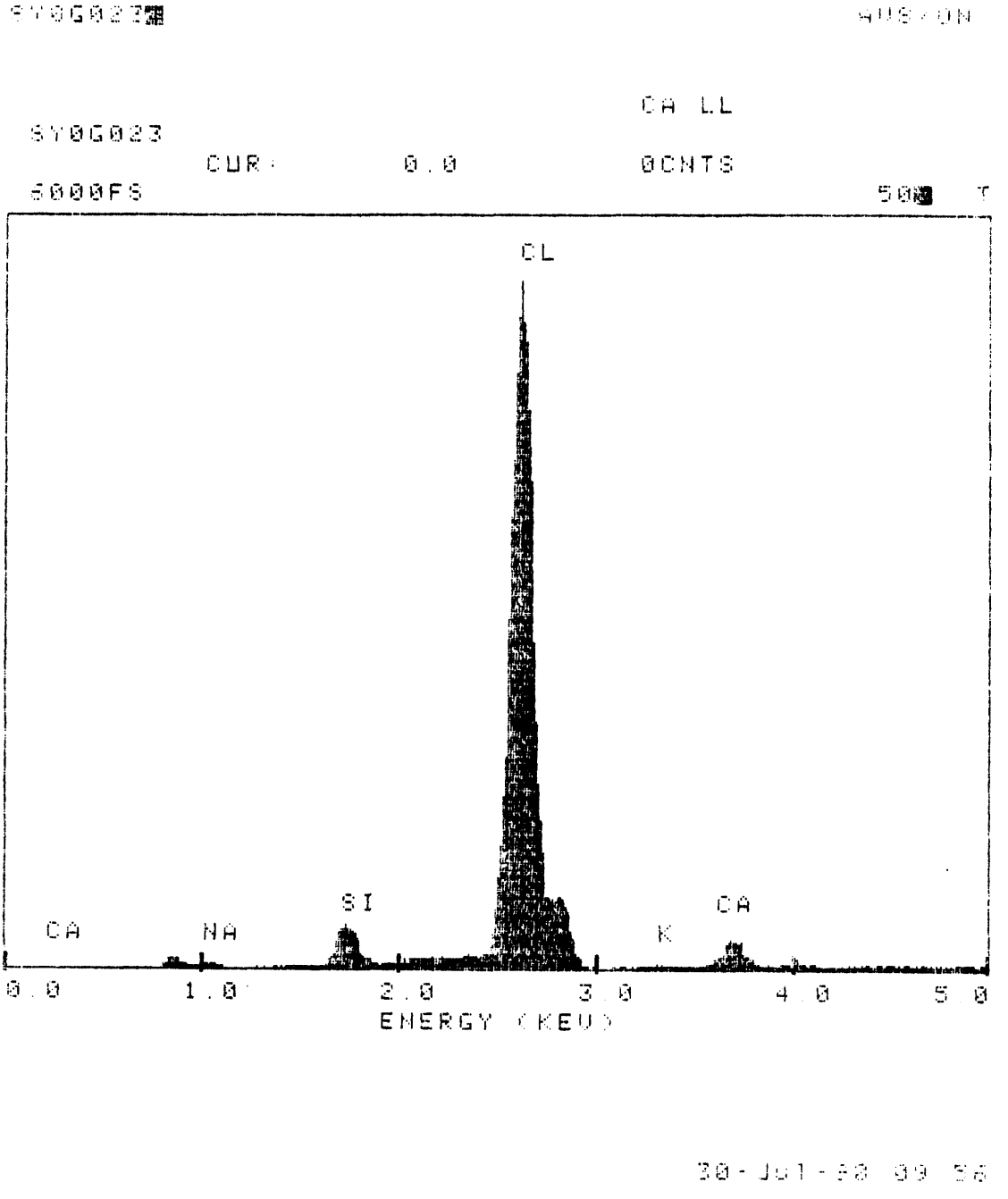

Figure A-13. Results from EDS analysis for high current density cathode, SEM given in **Figure** 3-3.

Sample 3-3

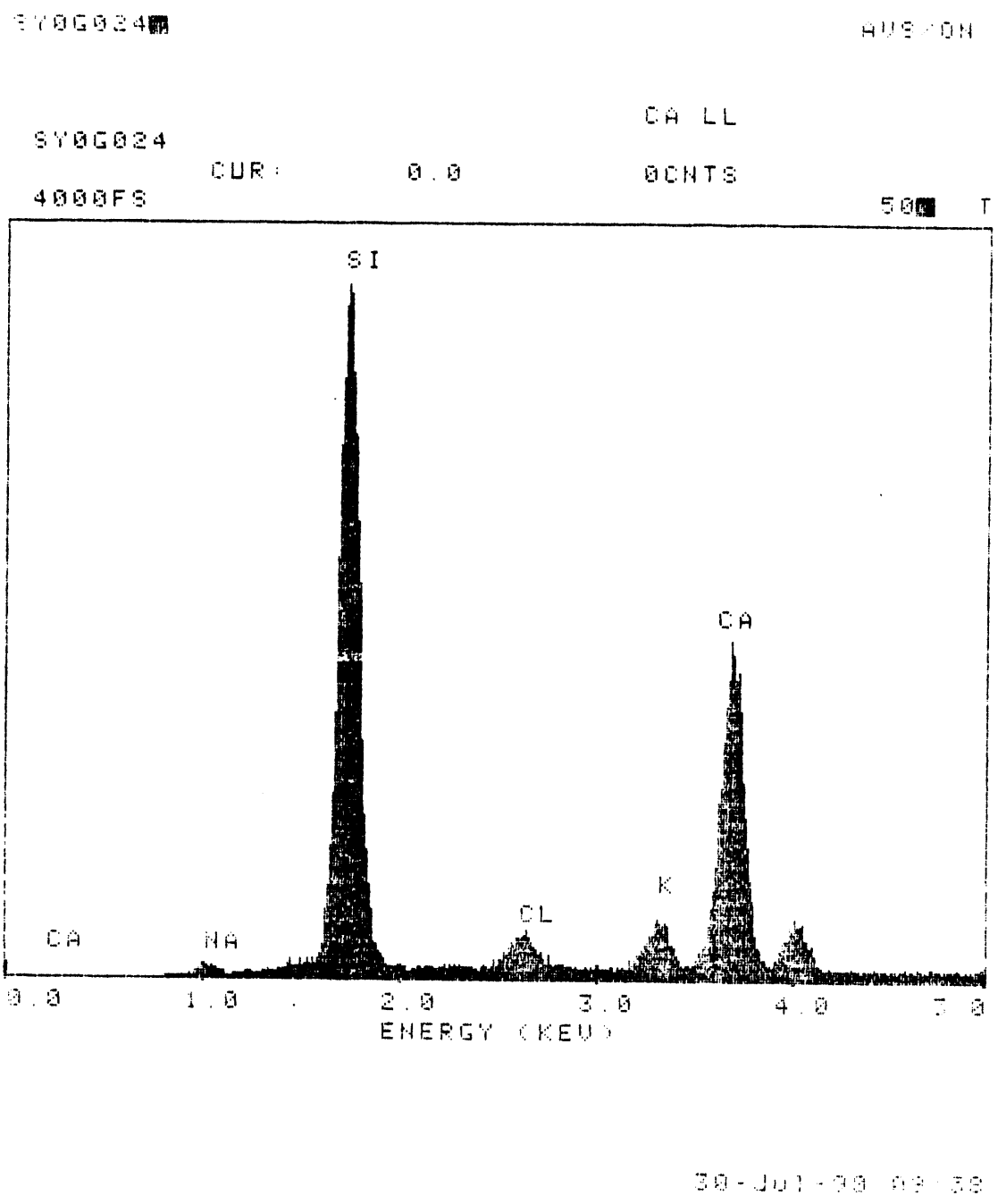

Figure A-14. Results from EDS analysis for high current density, SEM given in Figure 3-3.

Sample 3-3

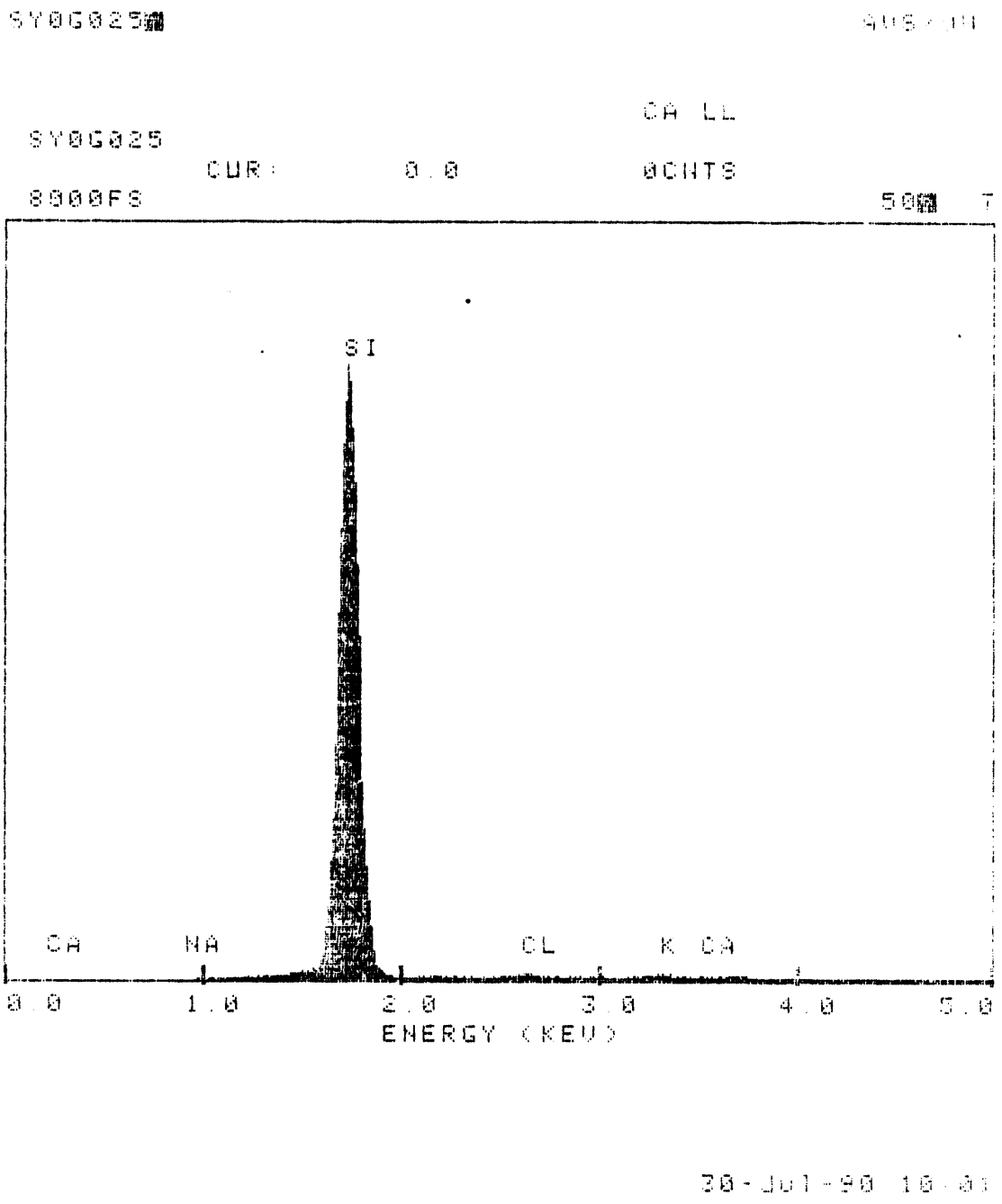

Figure A-15. Results from EDS analysis for samples recovered from the ground, SEM given in ground figure.

Sample ground

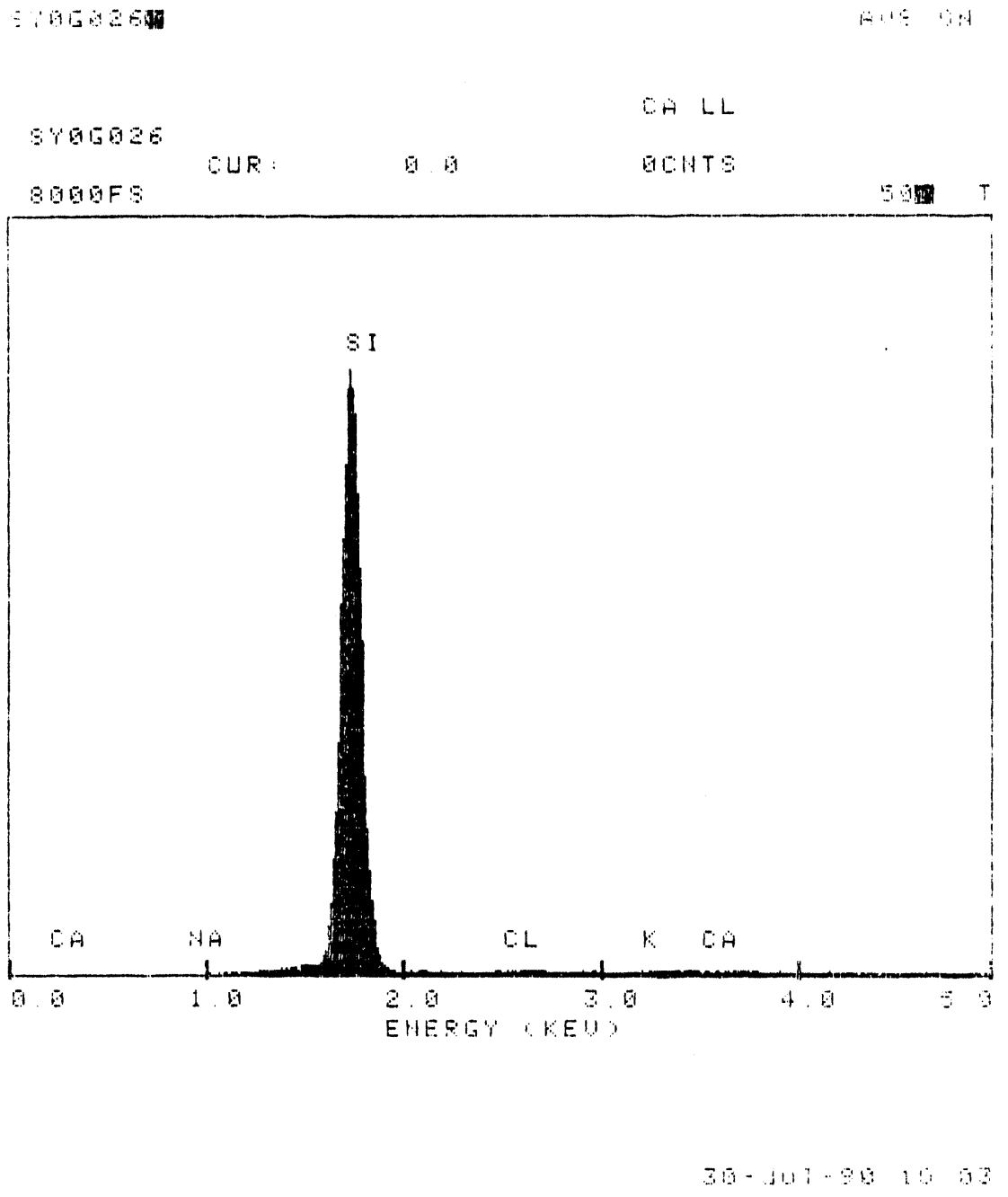

Figure A-16. Results from EDS analysis for samples recovered from the ground, SEM given in ground figure.

Sample ground

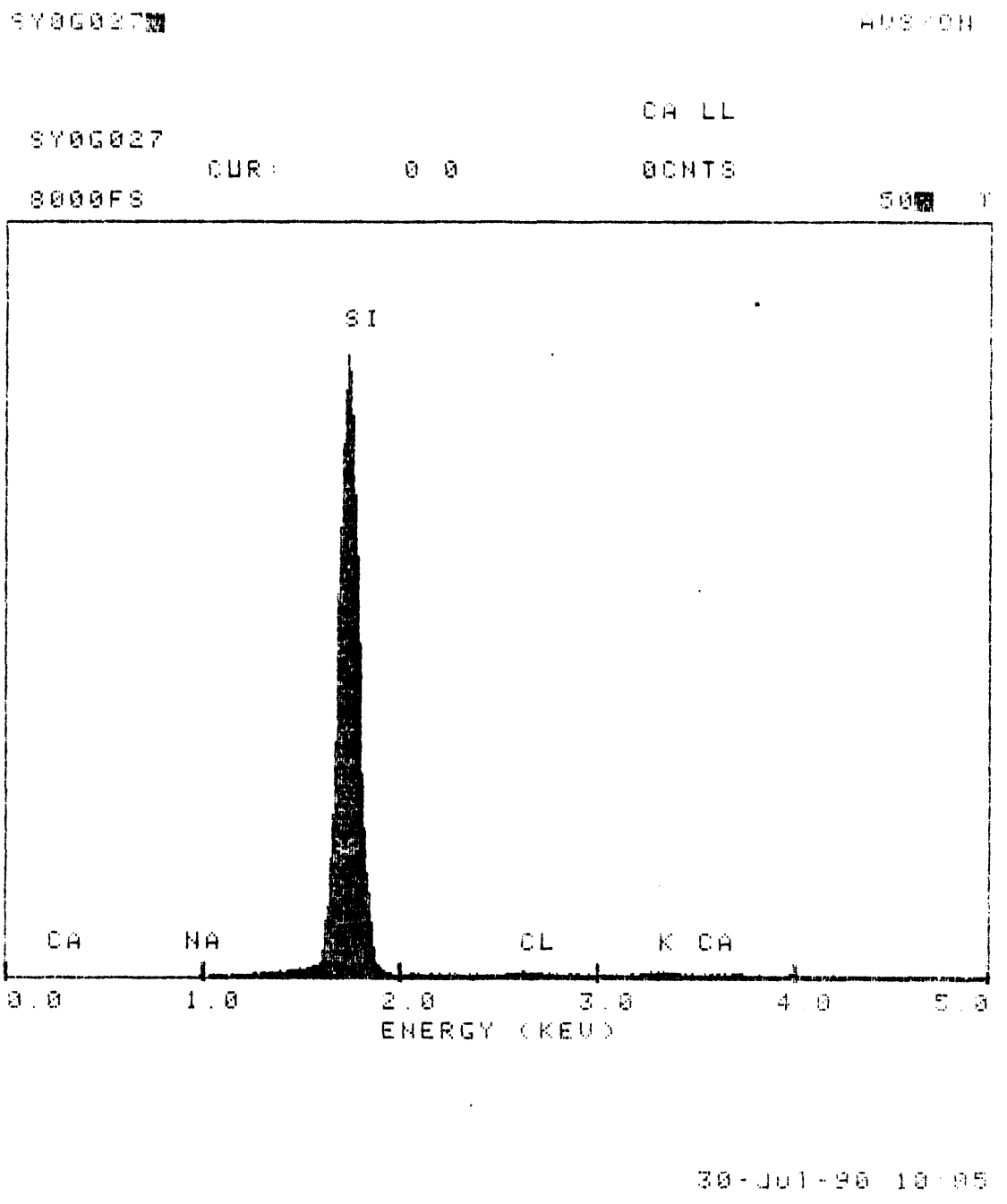

Figure A-17. Results from EDS analysis for samples recovered from the ground, SEM given in ground figure.

Sample ground

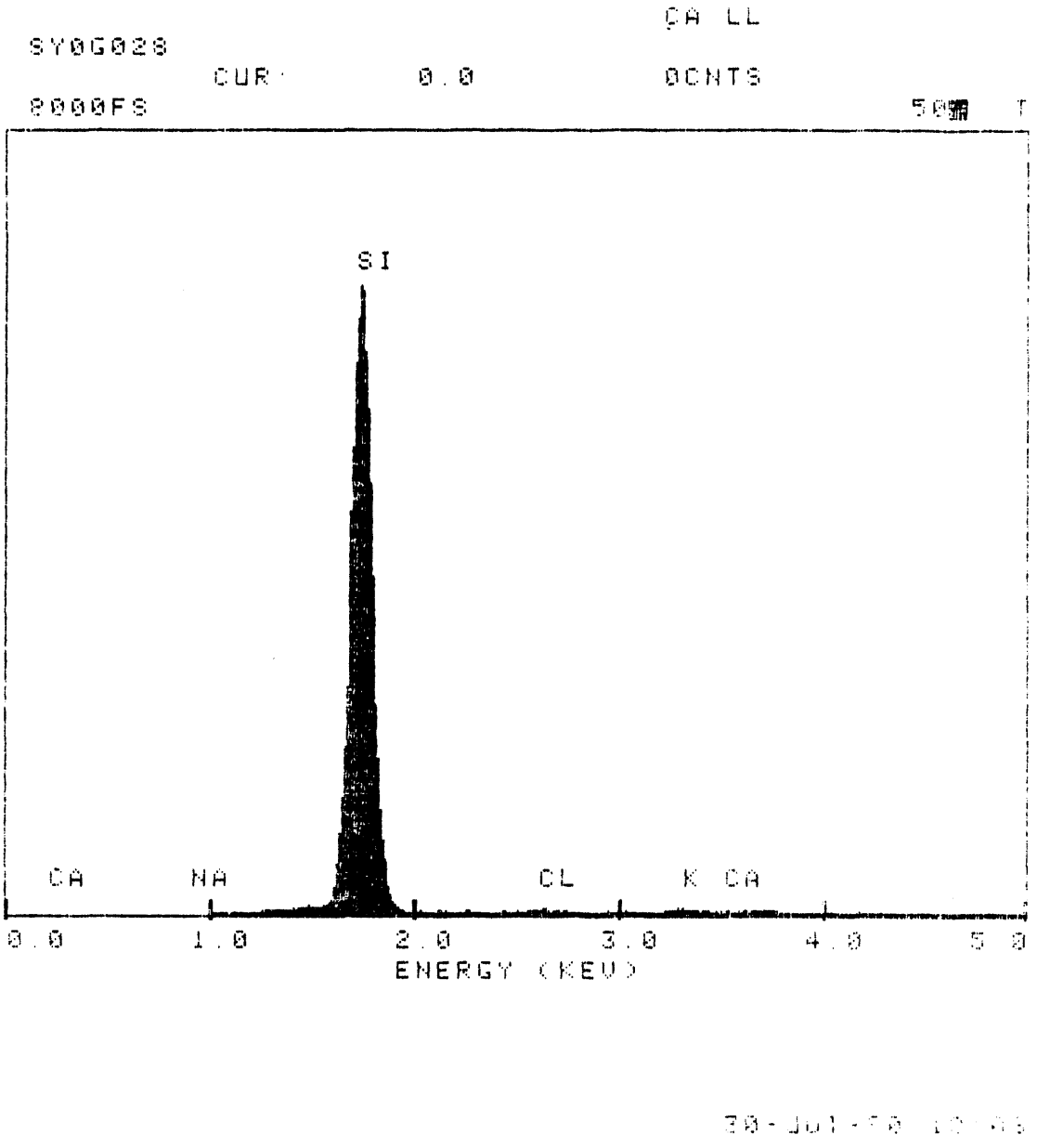

Figure A-18. Results from EDS analysis for samples recovered from the ground, SEM given in ground figure.

Sample ground

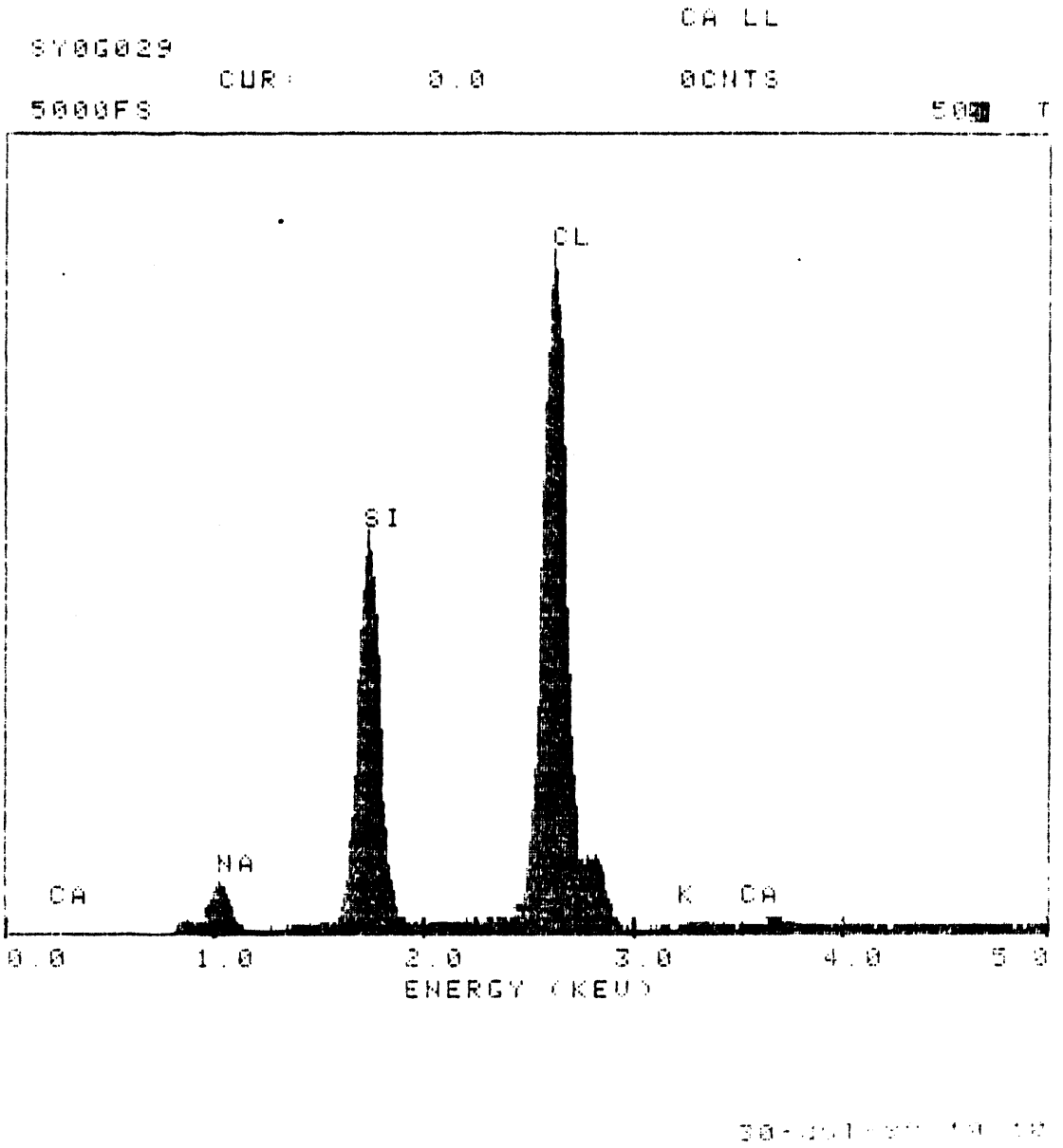

Figure A-19. Results from EDS analysis for samples recovered from the tank, SEM given in tank figure.

Sample tank bottom

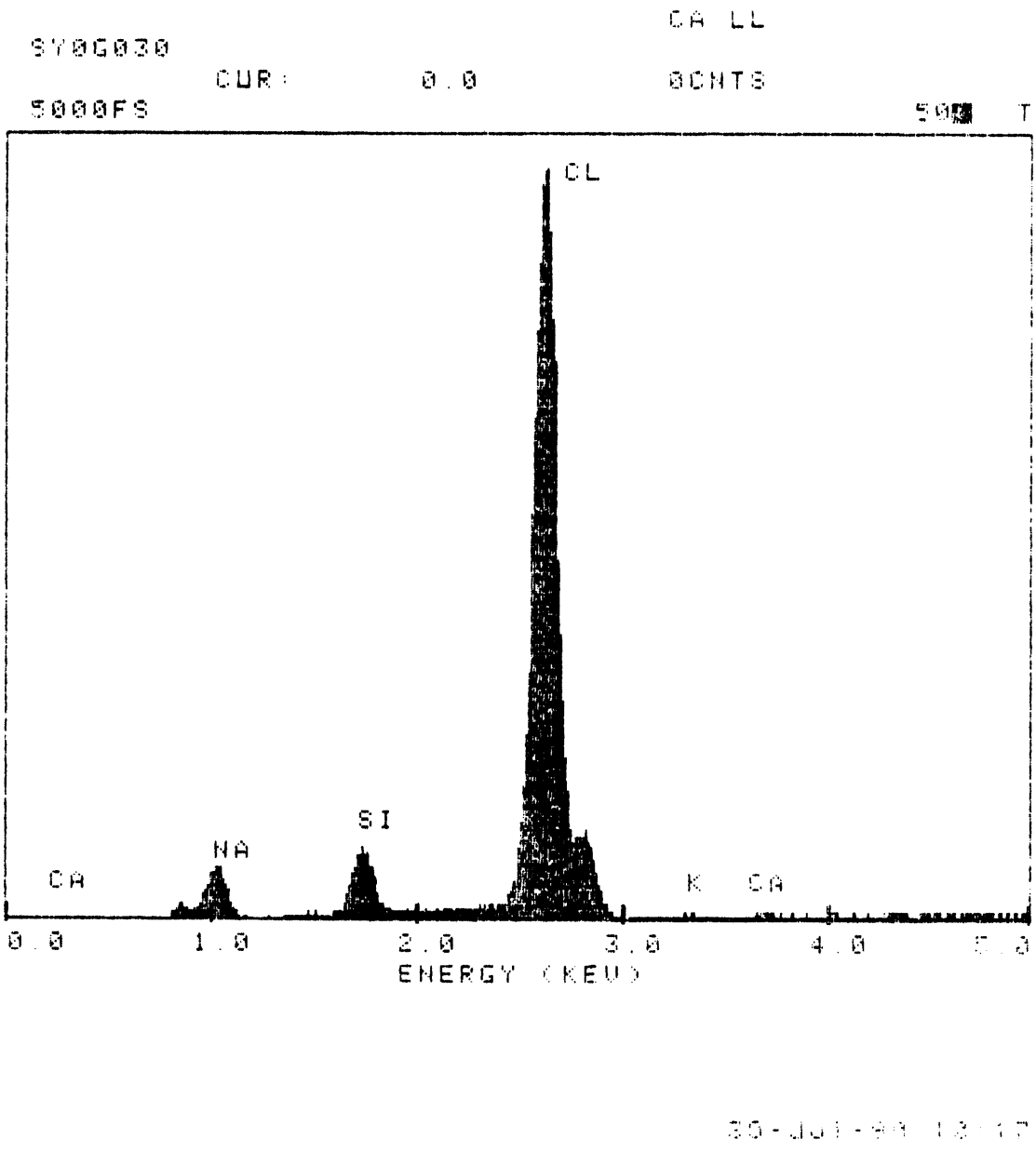

Figure A-20. Results from EDS analysis for samples recovered from the tank, SEM given in tank figure.

Sample tank bottom

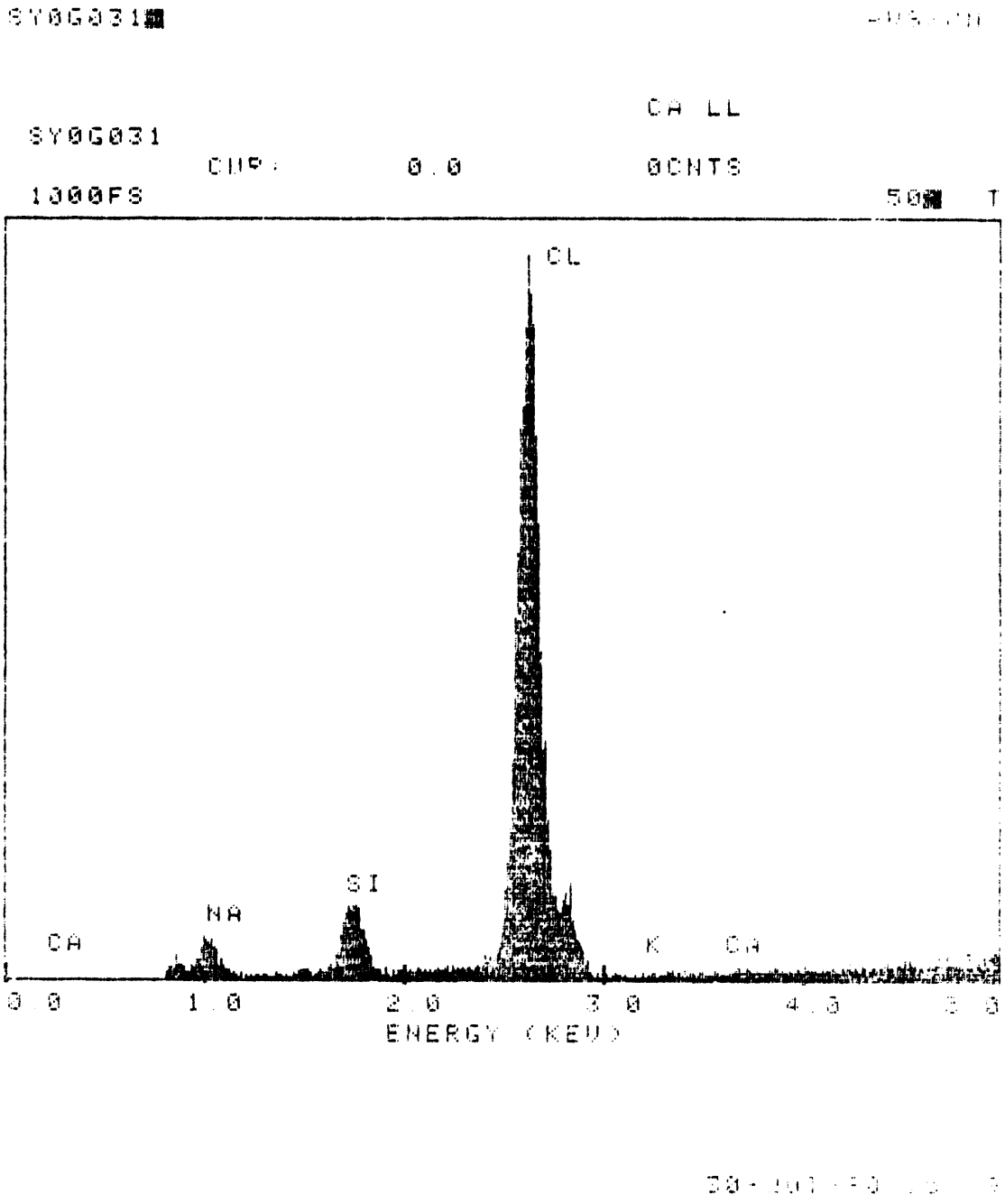

Figure A-21. Results from EDS analysis for samples recovered from the tank, SEM given in tank figure.

Sample tank bottom

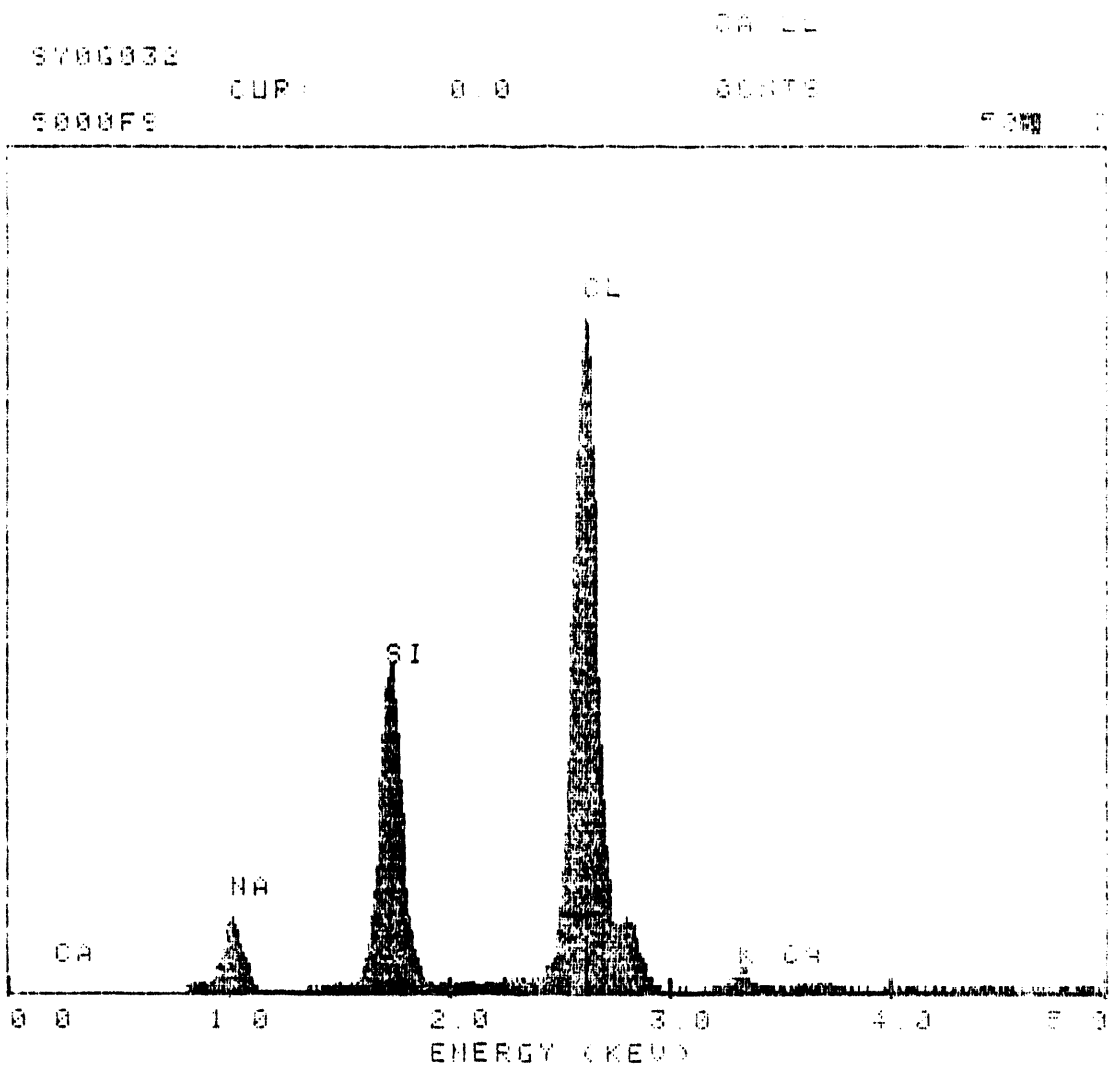

Figure A-22. Results from EDS analysis for samples recovered from the tank, SEM given in tank figure.

Sample tank bottom

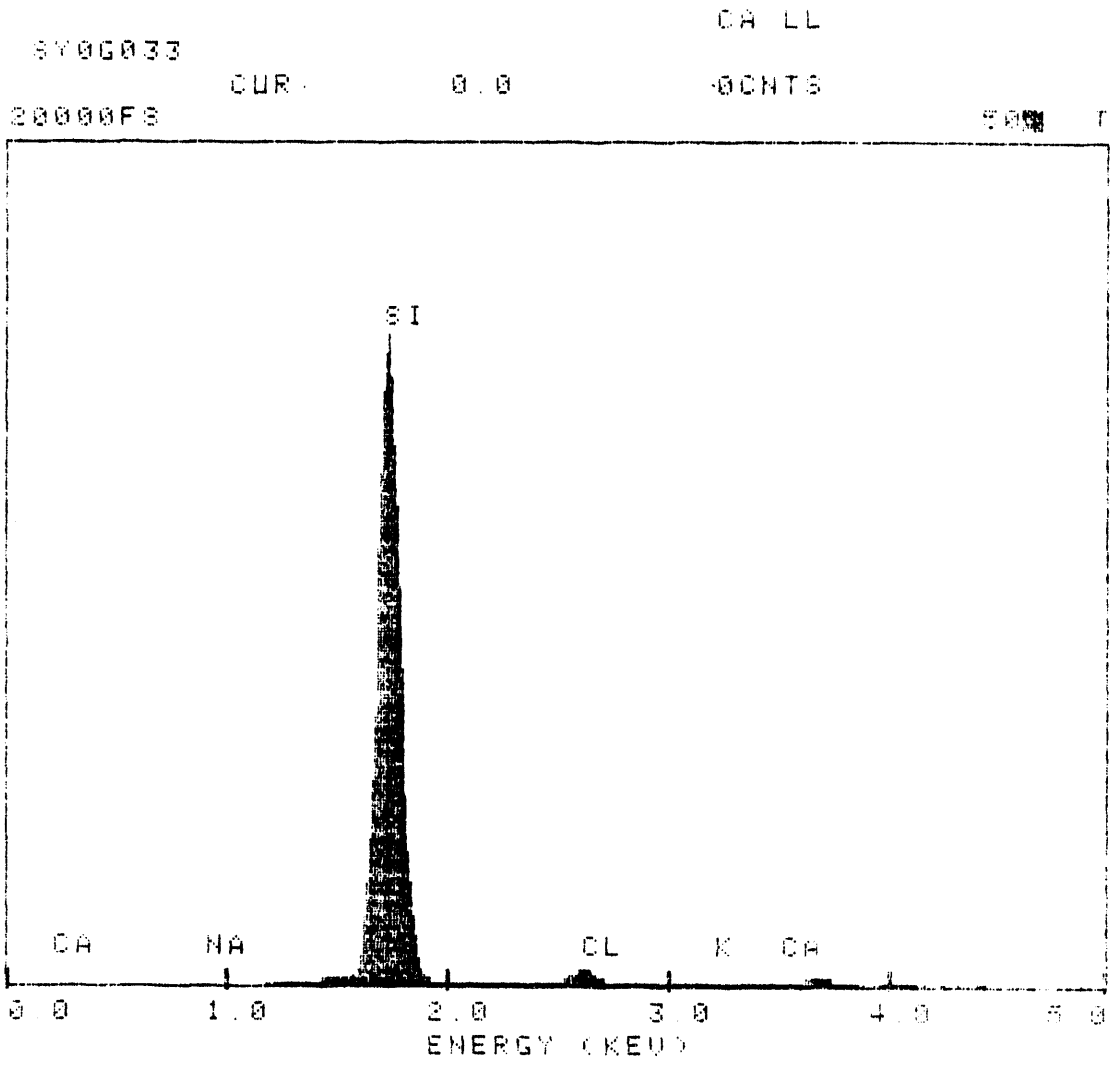

Figure A-23. Results from EDS analysis for samples recovered from the tank, SEM given in tank figure.

Sample tank bottom

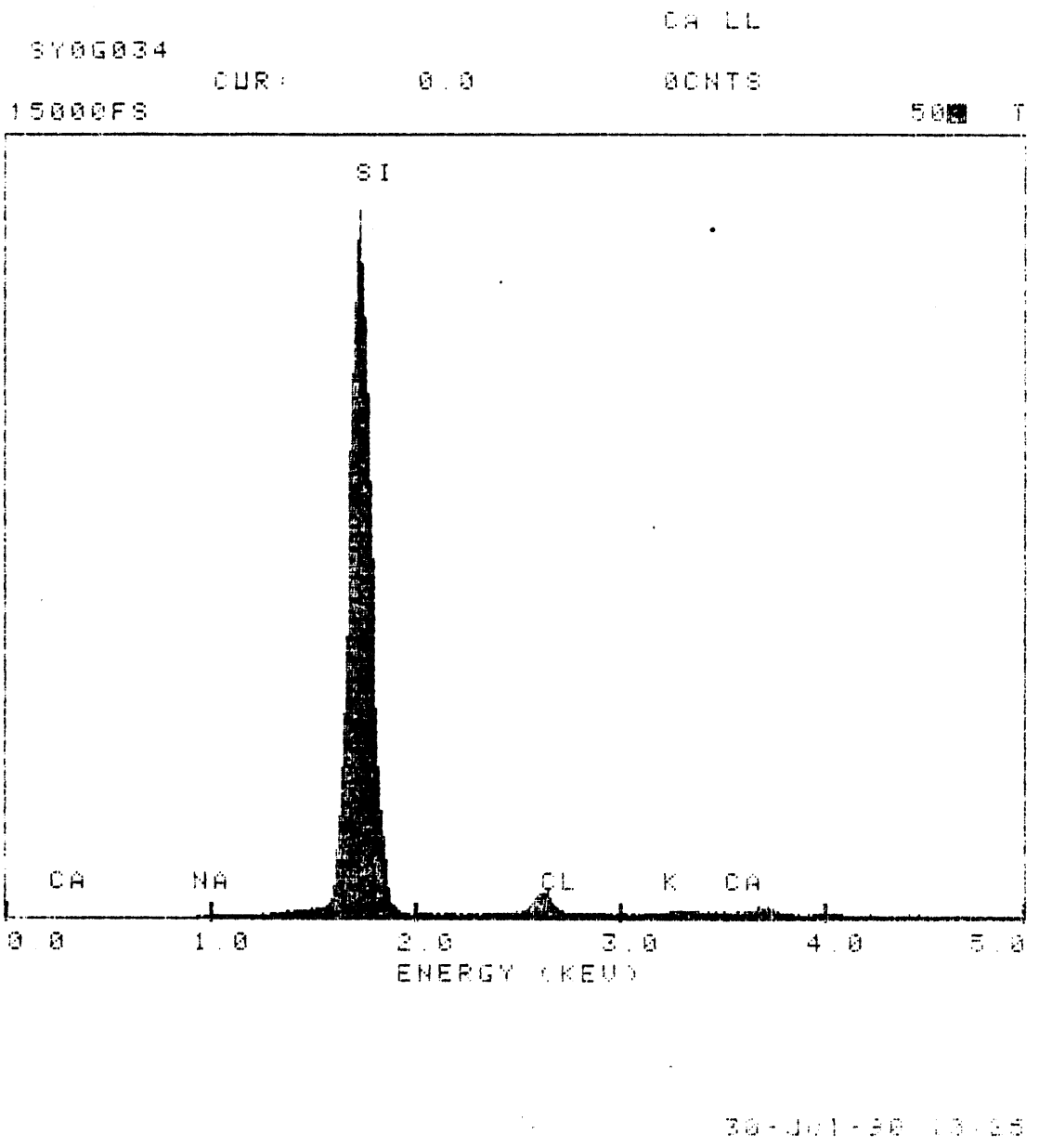

Figure A-24. Results from EDS analysis for samples recovered from the tank, SEM given in tank figure.

Sample tank bottom

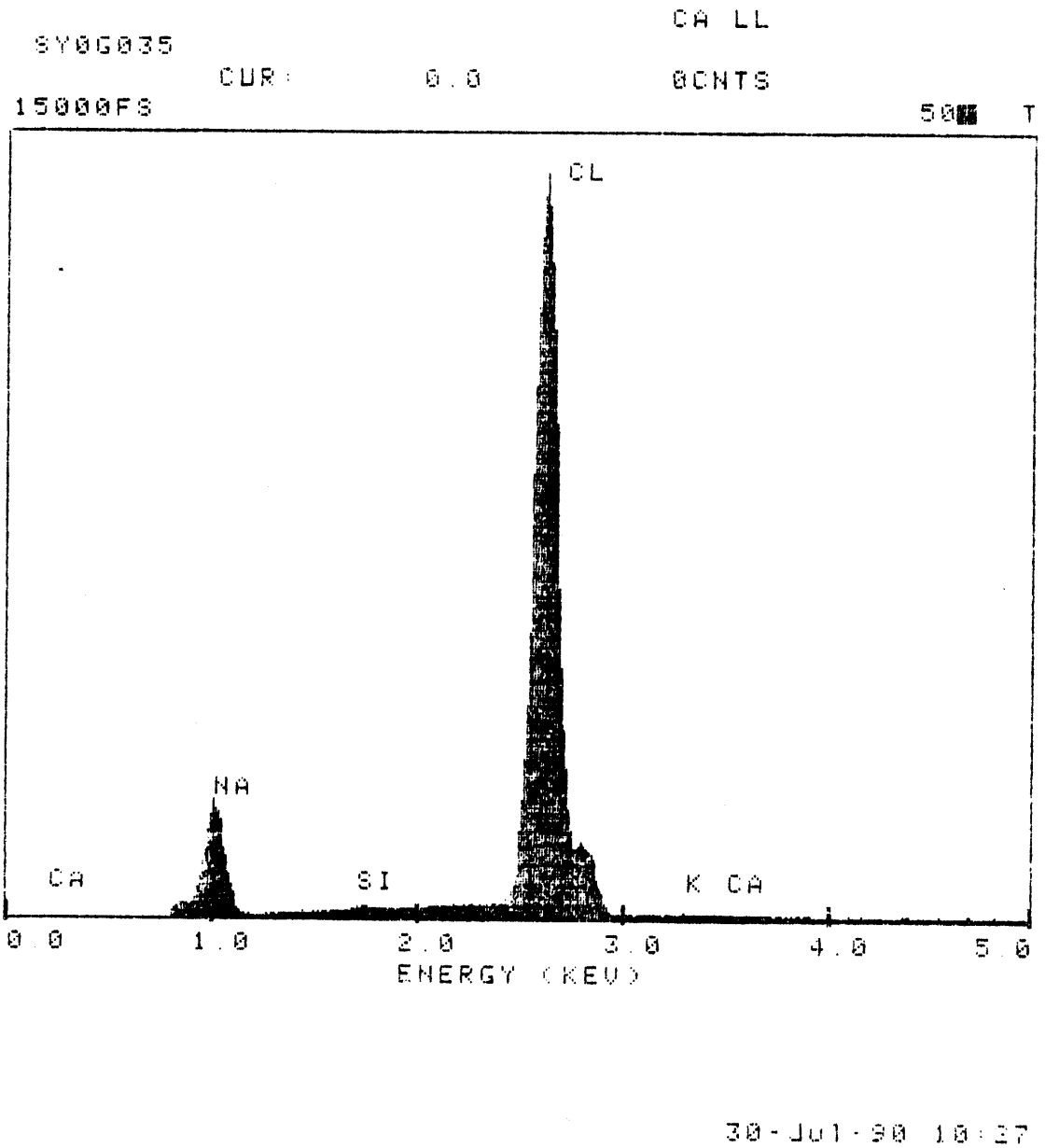

Figure A-25. Results from EDS analysis for samples recovered from the tank, SEM given in tank figure.

Sample tank bottom

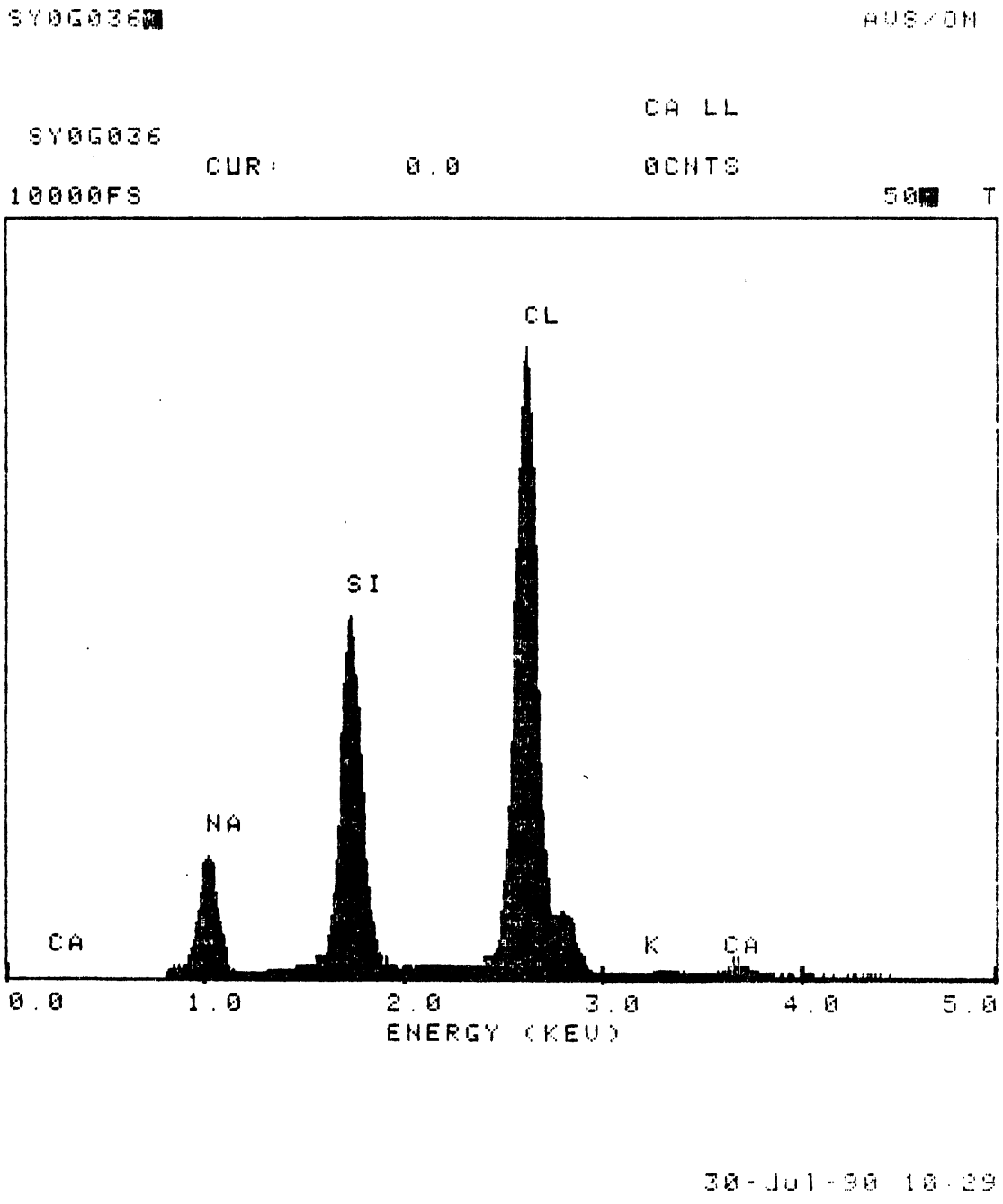

Figure A-26. Results from EDS analysis for samples recovered from the tank, SEM given in tank figure.

Sample tank bottom

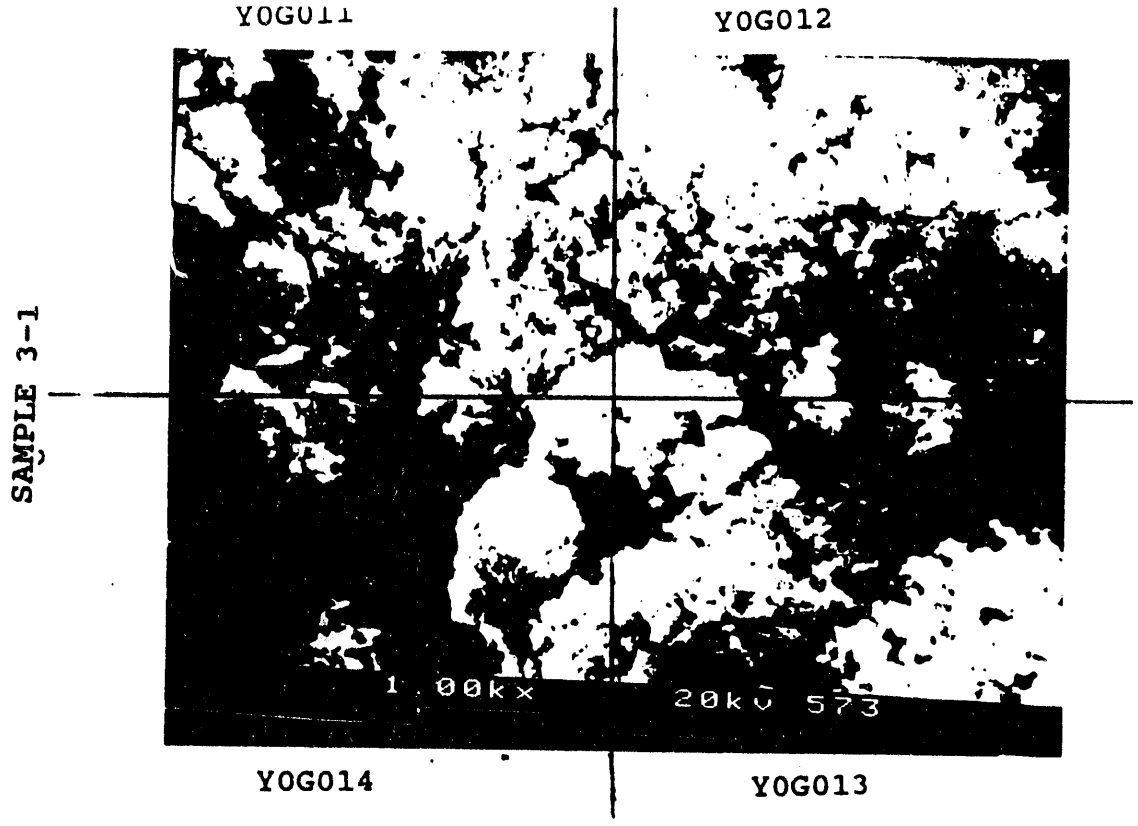

Figure A-27. Scanning Electron Microscopy (SEM) results for material deposited on cathode 1, lowest current density.

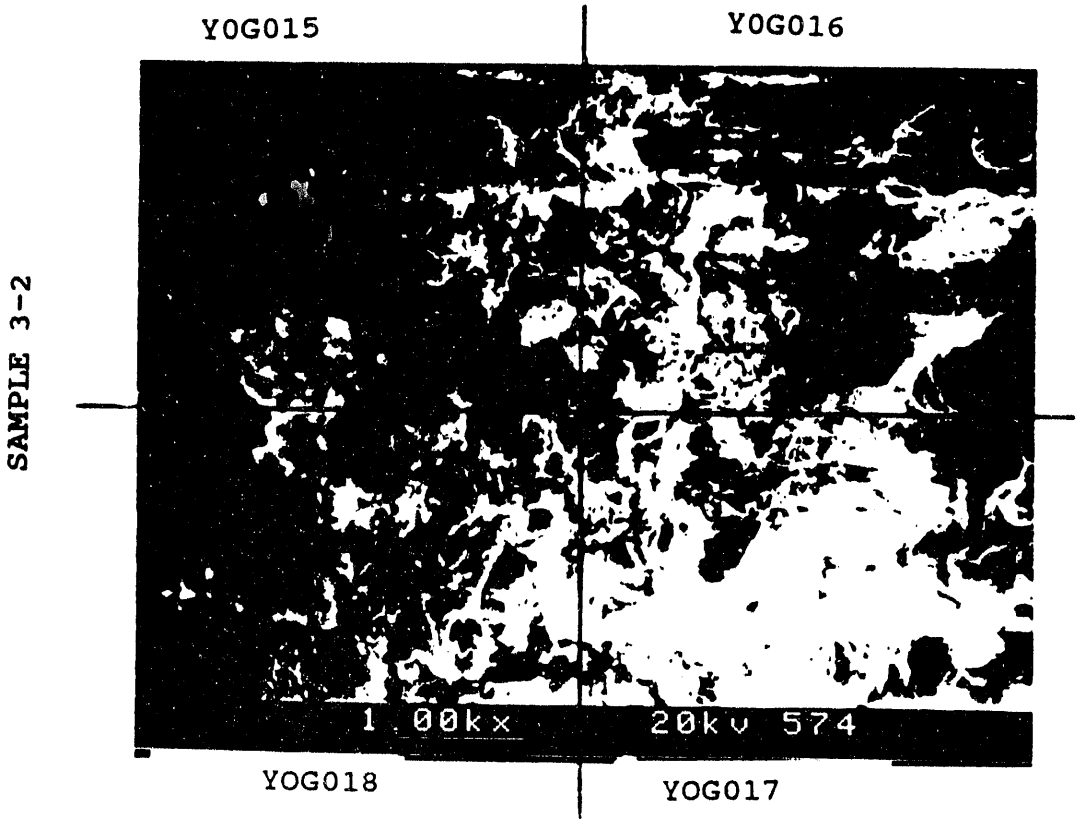

Figure A-28. Scanning Electron Microscopy (SEM) results for material deposited on cathode 2, medium current density.

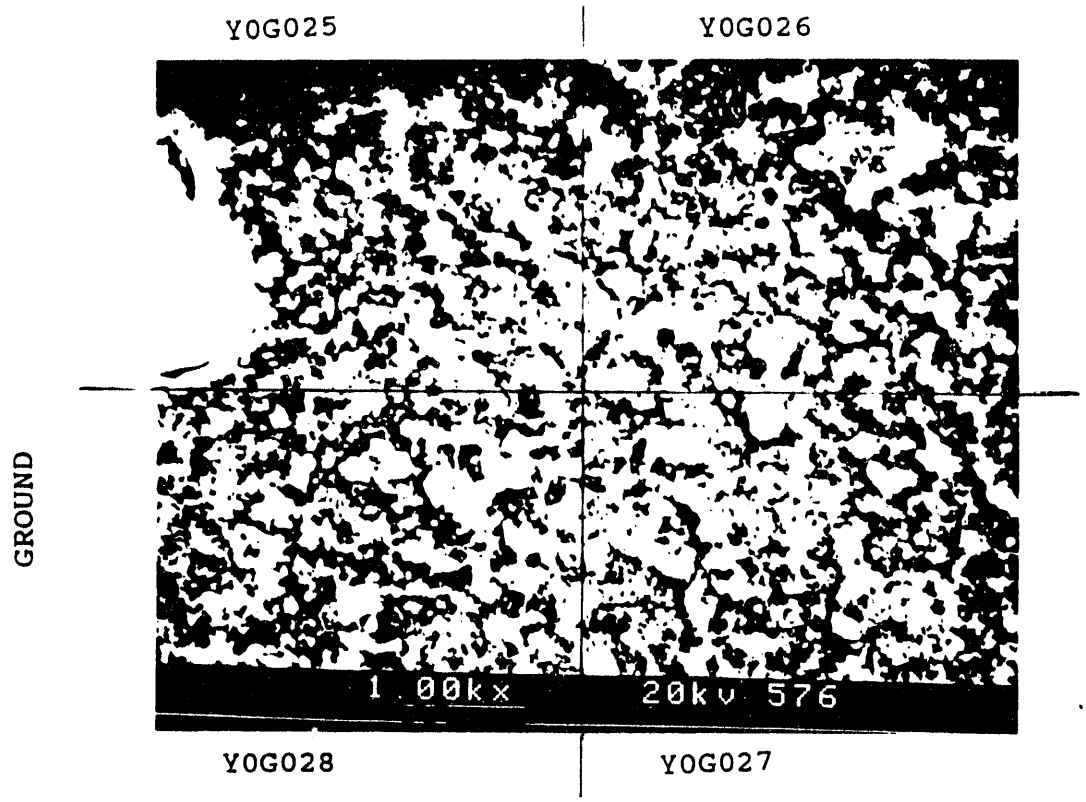

Figure A-29. Scanning Electron Microscopy (SEM) results from material recovered from the ground.

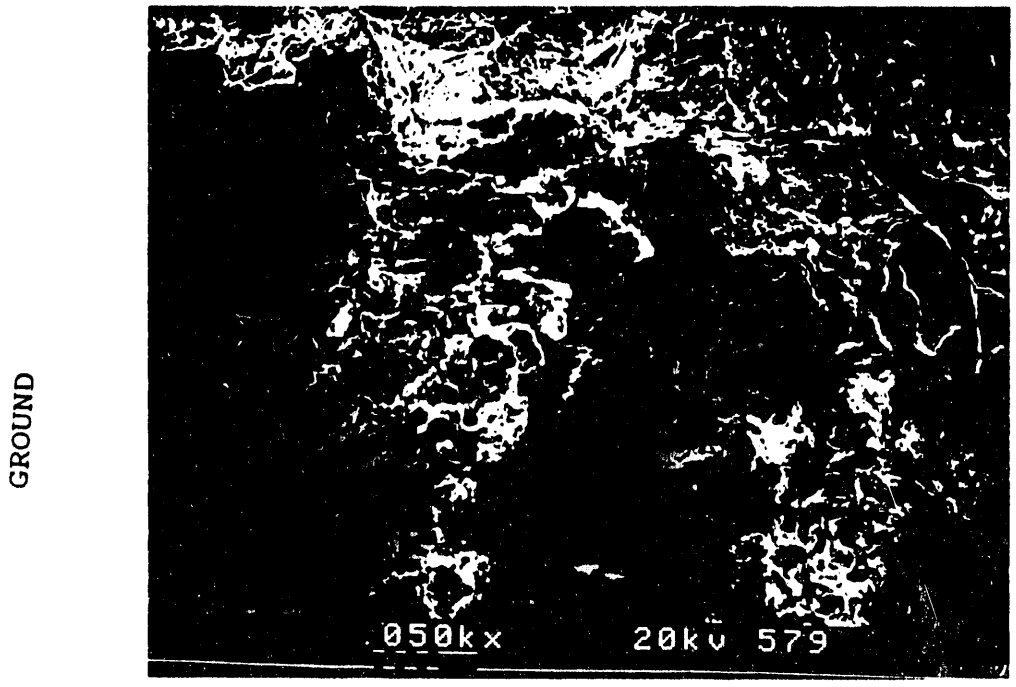

Figure A-30. Scanning Electron Microscopy (SEM) results from material recovered from the ground.

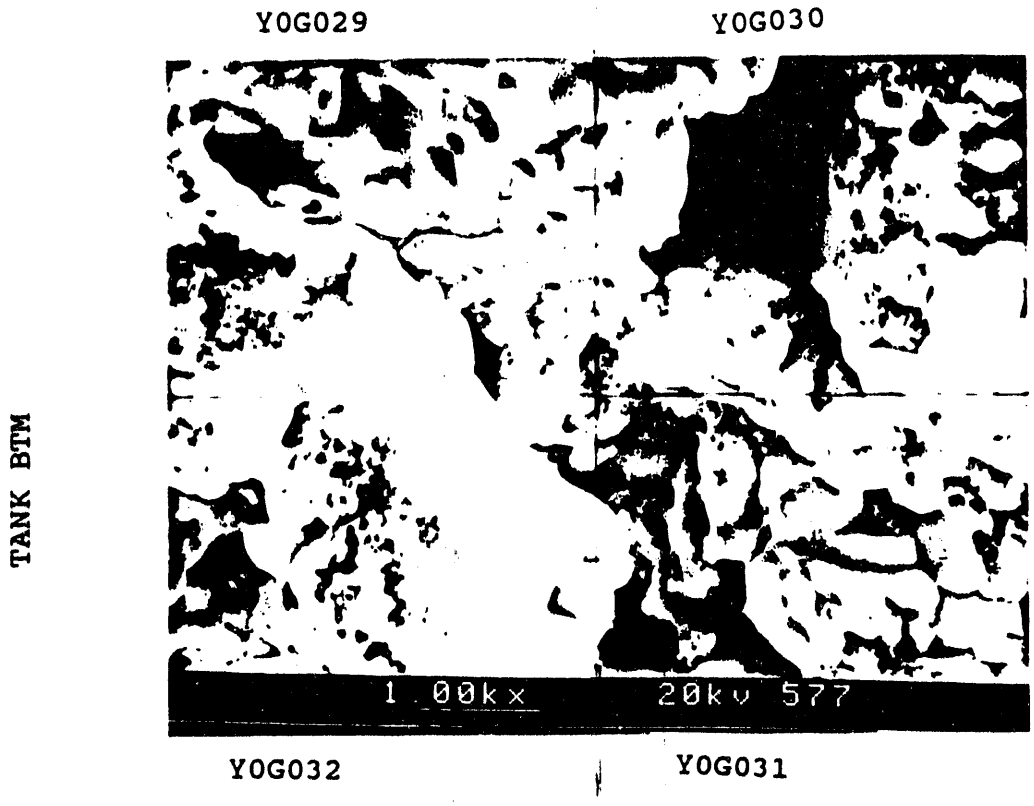

Figure A-31. Scanning Electron Microscopy (SEM) results from material recovered from the tank.

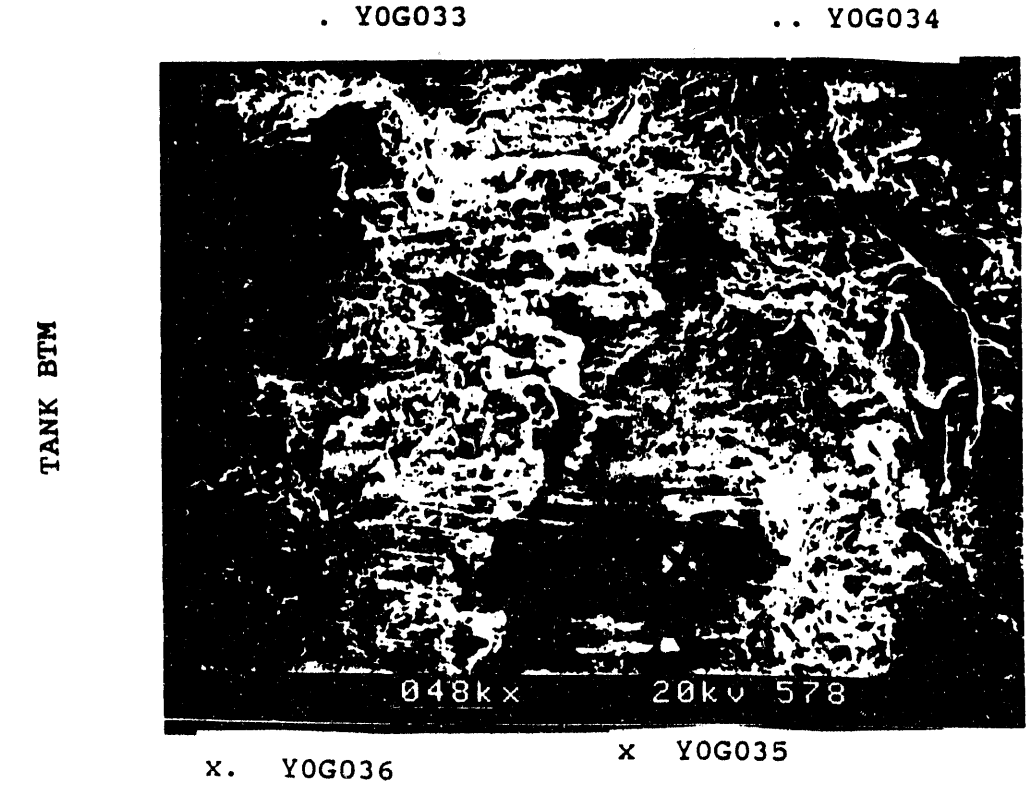

Figure A-32. Scanning Electron Microscopy (SEM) results from material recovered from the tank.

APPENDIX B

X-RAY DIFFRACTION RESULTS

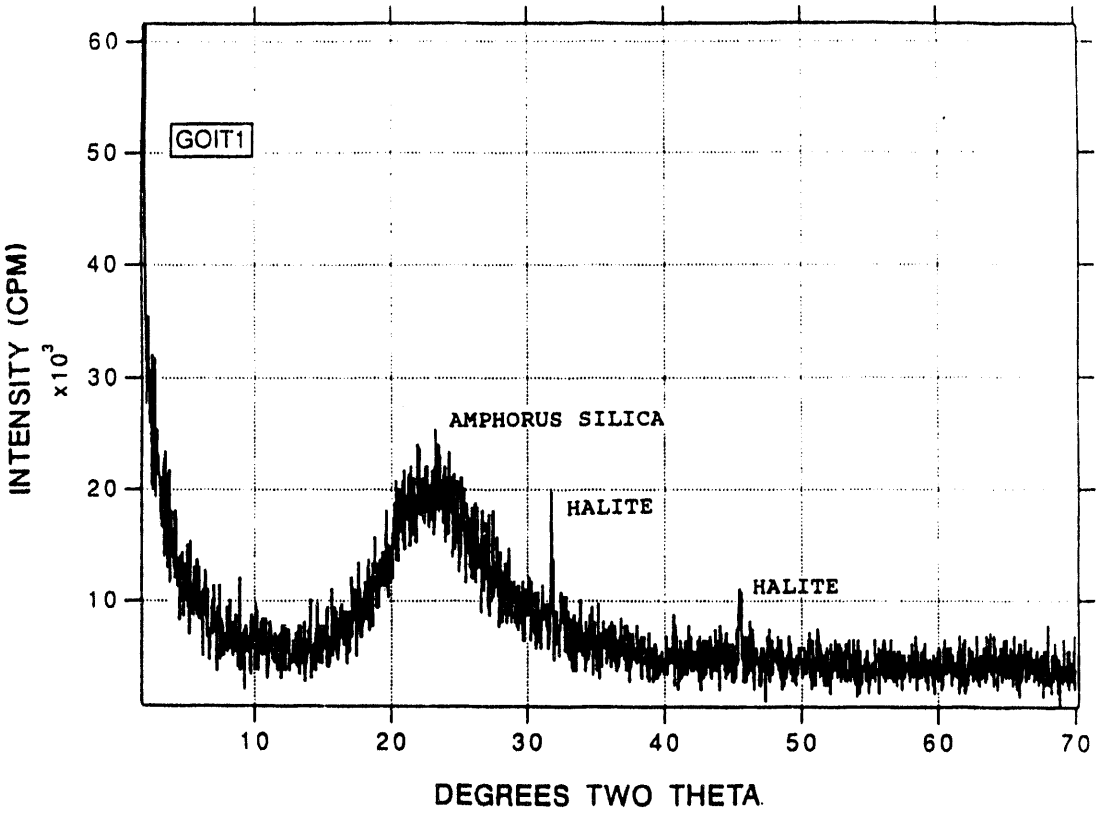

Figure B-1. Scanning Electron Microscopy (SEM) results from material deposited on cathode 1, lowest current density.

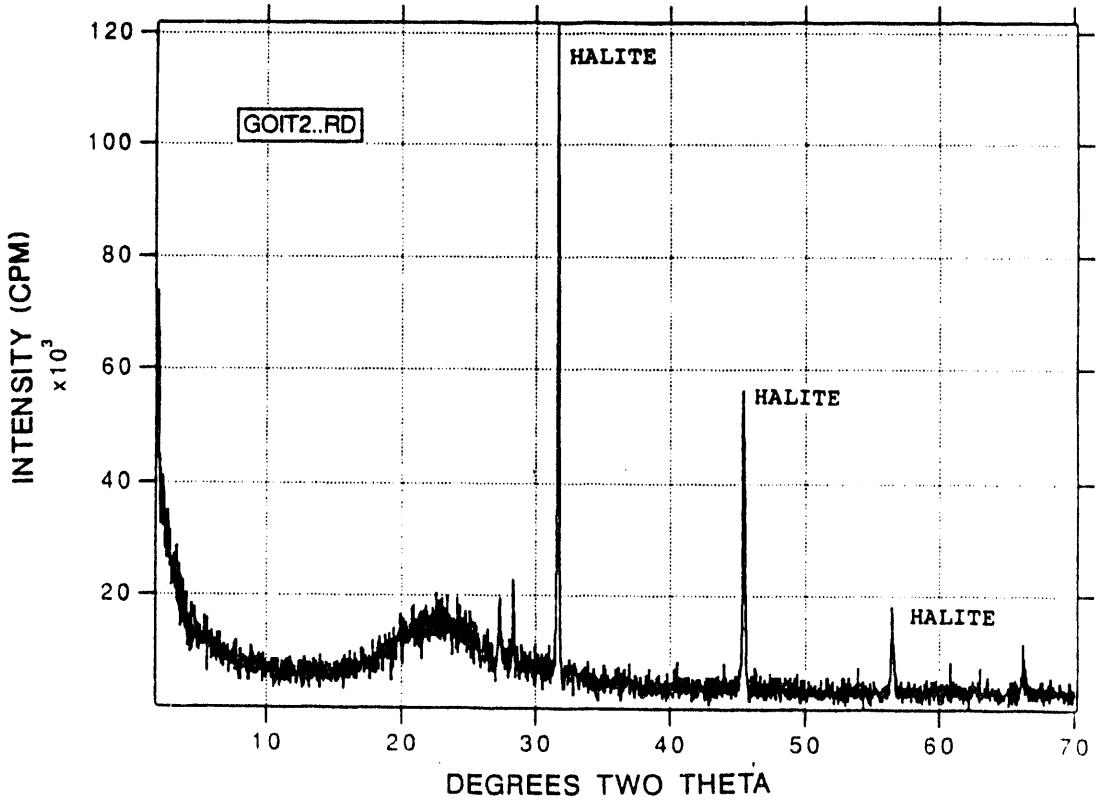

Figure B-2. Scanning Electron Microscopy (SEM) results from material deposited on cathode 2, medium current density.

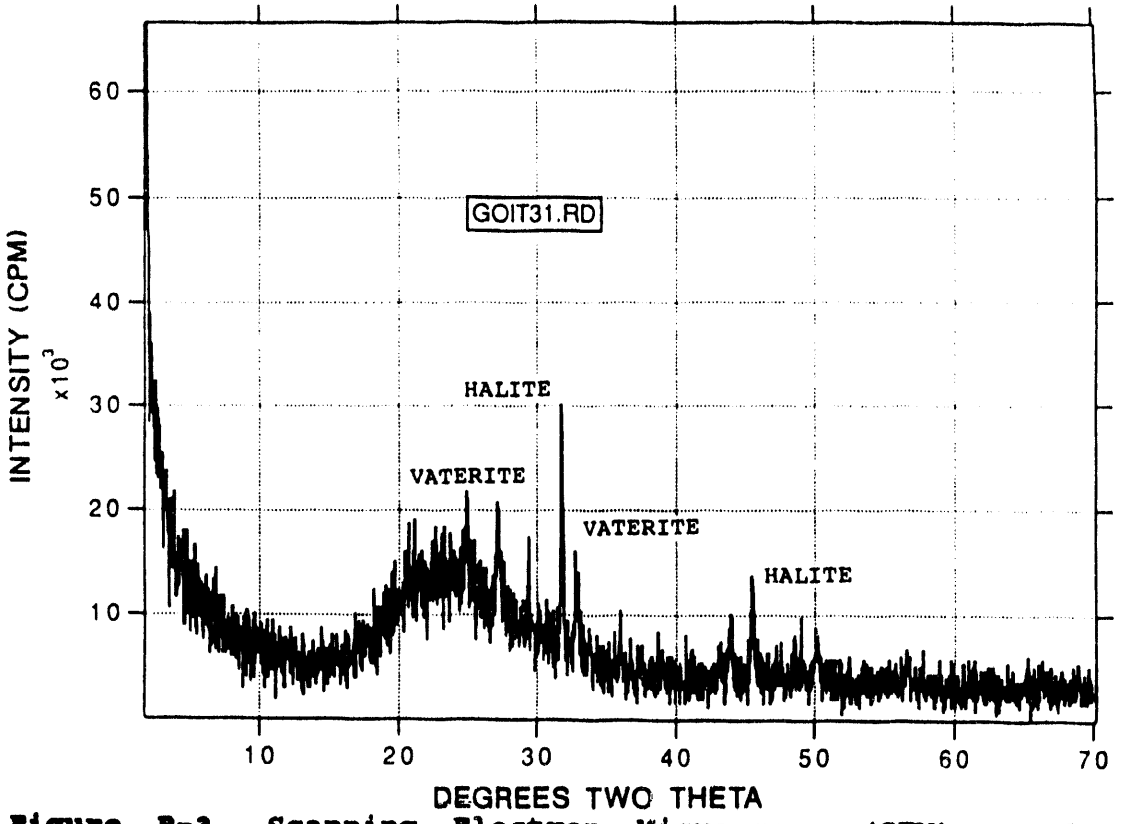

Figure B-3. Scanning Electron Microscopy (SEM) results from material recovered from the ground.

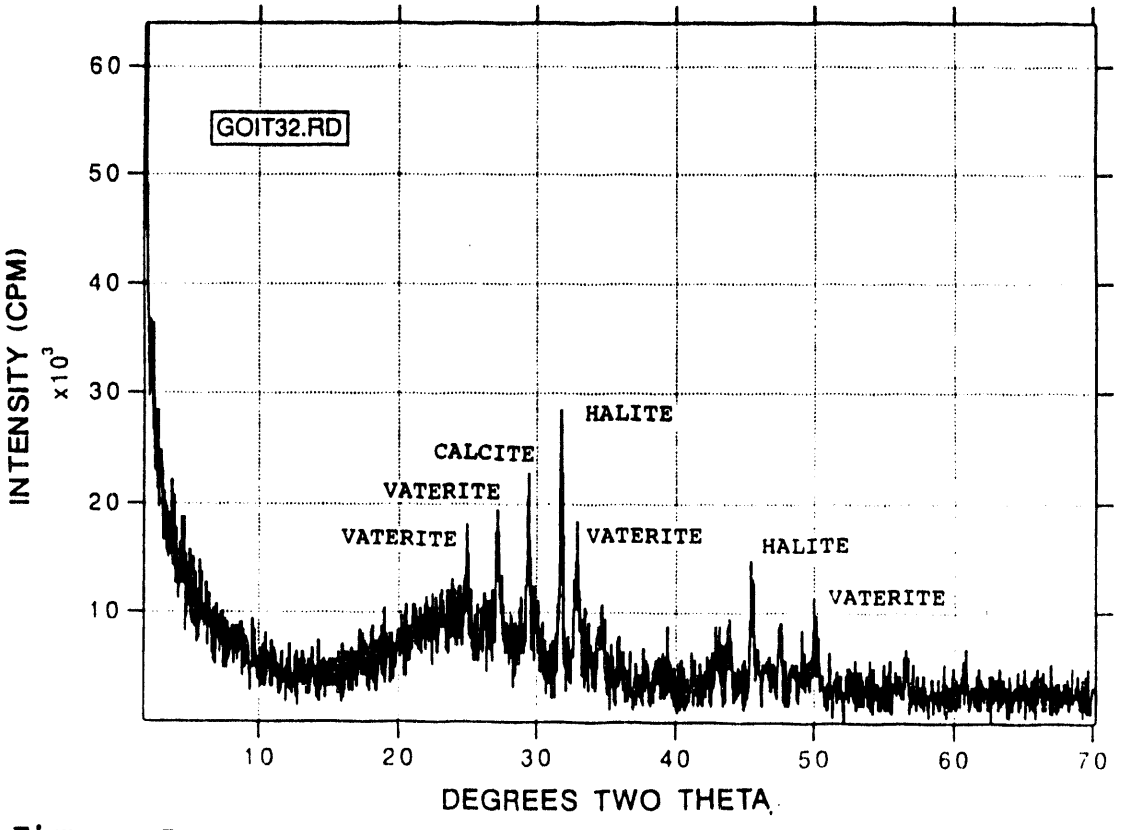

Figure B-4. Scanning Electron Microscopy (SEM) results from material recovered from tank.

END

DATE
FILMED
3/22/94